Journal of Petroleum Science and Engineering 213 (2022) 110377

Contents lists available at ScienceDirect

Journal of Petroleum Science and Engineering

journal homepage: www.elsevier.com/locate/petrol

# A new experimental method for comparing solvents in steam-solvent coinjection for bitumen recovery under controlled thermodynamic conditions

Kai Sheng [a], Hassan Amer [a], Young Liu [a], Ryosuke Okuno [a,*], Abdullah Al-Gawfi [b], Petro Nakutnyy [b], Kazunori Nakagawa [c]

[a] The University of Texas at Austin, USA
[b] Saskatchewan Research Council, Canada
[c] Japan Canada Oil Sands, Canada

ARTICLE INFO

*Keywords:*
Steam-assisted gravity drainage
Bitumen
Steam-solvent coinjection
Soaking
Dispersion

ABSTRACT

Solvent-aided steam-assisted gravity drainage (SA-SAGD) involves the interplay between phase behavior and fluid flow near the edge of a steam chamber, which affects the mixing of solvent with bitumen. The mixing of solvent with bitumen (i.e., dispersion) results in dilution of the bitumen and can improve the energy efficiency of SAGD. However, it is often difficult to analyze this complex interplay through large-scale steam injection experiments because of the transient chamber-edge thermodynamic conditions.

This paper presents an experimental program that compares the bitumen gravity drainage with steam injection (SAGD) and solvent-steam co-injection (SA-SAGD) under controlled thermodynamic conditions. In addition to SAGD as the base case, two sets of SA-SAGD were performed with 20 mol% $C_4$ and 10 mol% $C_8$ in the coinjected vapor at 3500 kPa. The experiments used a sand-pack of 3-inch diameter and 15-inch length, which was placed in a 25-L cylindrical pressure vessel. The sand-pack was surrounded by one-inch annular space, into which the vapor phase was injected under controlled pressure, temperature, and composition. Oil production and temperature profiles inside and outside the sand-pack were recorded for all experiments. Excavated samples from the sand-pack were analyzed after the experiments.

The total recovery factors for SAGD, $C_4$-SAGD, and $C_8$-SAGD were 78%, 84%, and 89%, respectively. The recovery factors at 1 h for SAGD, $C_4$-SAGD, and $C_8$-SAGD were 71%, 80%, and 85%, respectively. The peak oil rate was 9.8 $cm^3$/min with SAGD, 14.6 $cm^3$/min with $C_4$-SAGD, and 31.3 $cm^3$/min with $C_8$-SAGD. The SA-SAGD cases resulted in markedly better results than the SAGD case, and $C_8$-SAGD yielded more rapid oil drainage than $C_4$-SAGD.

The SAGD experimental data were history-matched using a numerical simulation model. Based on the calibrated numerical model, the SA-SAGD experimental data were history-matched by adjusting the dispersion coefficient to model the mixing between the solvent and bitumen. The apparent dispersion coefficients for $C_4$ and $C_8$ in bitumen were determined to be 0.012 $m^2$/day and 0.093 $m^2$/day, respectively. The experimental program verified in this research offers a way to systematically compare different solvents for SA-SAGD with their quantifiable dispersion coefficients under given chamber conditions.

## 1. Introduction

Steam-assisted gravity drainage (SAGD) is one of the most widely used methods for thermal recovery of extra-heavy oil or bitumen. Solvent-aided, steam-assisted gravity drainage (SA-SAGD) attempts to enhance the efficiency of SAGD by coinjecting solvent, usually a mixture of n-alkanes or pure n-alkanes, along with steam. In both SAGD and SA-SAGD, stacked horizontal well-pairs are drilled into the formation. The upper well injects the steam and solvent, while the lower well produces oil and water by gravity.

* Corresponding author. Department of Petroleum and Geosystems Engineering, The University of Texas at Austin, 200 E. Dean Keeton Street, Stop C0300, Austin, TX, 78712, USA.
*E-mail address:* okuno@utexas.edu (R. Okuno).

https://doi.org/10.1016/j.petrol.2022.110377
Received 15 October 2021; Received in revised form 26 February 2022; Accepted 3 March 2022
Available online 5 March 2022
0920-4105/

SA-SAGD has the potential to reduce heat losses by decreasing the vapor phase temperature (Keshavarz et al., 2014, 2015; Li et al., 2011a, 2011b; Nasr et al., 2003) and by speeding up the oil production due to dilution. As a result, SA-SAGD methods produce more bitumen for the same amount of steam input, lowering the steam to oil ratio (SOR).

Although SA-SAGD methods have been studied using laboratory experiments and simulations, the complex phenomena are still to be understood, such as the condensation and the mass transfer of solvent in the porous medium and the effect of solvent dispersion on oil recovery under controlled thermodynamic conditions. Large-scale experiments and field data of SAGD and SA-SAGD provide important data of transient mass and energy balances. However, it is difficult to confirm detailed mechanisms that occur through the interplay between phase behavior and gravity drainage in SA-SAGD. For example, chamber-edge conditions should be influential to the gravity drainage along the edge of a steam chamber because they are the boundary conditions for the mixing of solvent with bitumen. However, such boundary conditions vary with time in a way that is indefinite, but specific to the experimental conditions. This inherent limitation in the large-scale experiments is addressed by more precisely controlled experiments at a small scale in this paper. This paper's novelty lies in the newly designed experimental program and its verification using SAGD and SA-SAGD.

There are many physical experiments of SAGD and SA-SAGD, ranging from larger-scale sand-packs to micro-scale models. One of the earliest SAGD experiments was performed by Butler (1994), where a sand-pack 2-D model was used. Later, Yazdani and Maini (2005) and Moghadam et al. (2009) used sand-pack porous media to study VAPEX. Co-injection of solvents with steam was studied in recent years; e.g., Ayodele et al. (2008), Deng et al. (2010), and Khaledi et al. (2012). More recently, Al-Murayri et al. (2016) investigated SA-SAGD using a large-scale sand-pack 2-D cross-section model. Sheng et al. (2021a) presented a 3-D physical model experiment of SA-SAGD with multi-component condensate. Their experimental setup used a 190-L cylindrical vessel. Haddadnia et al. (2018) and Zirahi et al., 2020a, 2020b presented a 2-D physical model experiment for steam and water-soluble solvents coinjection. As mentioned above, however, the substantially transient conditions for large-scale experiments were not convenient for a focused investigation into detailed compositional phenomena near the chamber edge.

In this research, small-scale experiments of SAGD and SA-SAGD were performed at Saskatchewan Research Council (SRC), Regina, Saskatchewan, Canada. The sand pack used had a pore volume of 520 $cm^3$ with a porosity of 33%, and the total experiment vessel had a volume of 25 L. This experimental method provided a convenient way to quickly test potential solvents in terms of condensation, bitumen dilution, and enhancement of oil flow at desired thermodynamic conditions. One test takes less than 5 h with less material and preparation work than large-scale steam-injection experiments.

For solvent to dilute bitumen requires the solvent dispersion in the oil phase. Hydrodynamic dispersion, widely known as dispersion, is the mixing of solvent during miscible displacements (Lake, 1989). Hydrodynamic dispersion has two components: molecular diffusion and mechanical dispersion. Molecular diffusion is caused by concentration gradients, while mechanical dispersion results from velocity variation under pore-scale heterogeneity (Pickens and Grisak, 1981). The mixing caused by hydrodynamic dispersion of solvent and bitumen in the porous medium in SA-SAGD is crucial to the evaluation of different solvents and their production forecast.

Solvent dispersion has been studied through a combination of experiments, analytical methods, and simulations. There is a limited amount of data specifically regarding the dispersion coefficient in SA-SAGD. However, solvent diffusion and dispersion in bitumen recovery were studied extensively for vapor-assisted petroleum extraction (VAPEX). The idea of VAPEX was developed by Butler and Mokrys (1991) to overcome shortcomings associated with the energy consumption by SAGD. It replaces steam injection with vapor solvent injection, and it lowers the viscosity of bitumen by dilution.

Nghiem et al. (2001) investigated dispersion and diffusion in VAPEX with propane using a compositional reservoir simulator. The dispersion coefficient used for propane was $5.04 \times 10^{-4}$ $m^2$/day, which was much larger than the molecular diffusion of propane in bitumen. The authors stated that the growth of the vapor chamber was controlled by molecular diffusion and convective dispersion, and showed that transverse dispersion was the dominant mechanism for the fluid mixing at the interface between solvent and heavy oil.

Dunn et al. (1989) studied gravity drainage of heavy oil by the injection of propane and butane. An analytical model for oil production was developed based on Butler and McNab's SAGD equation (Butler et al., 1981). The predicted cumulative oil production using their analytical model was much smaller than their experimental results. To history-match the experiment data, a large effective diffusion coefficient in the range of $10^{-2}$ $m^2$/day had to be used. This value was much greater than $10^{-5}$ $m^2$/day reported in the literature (Das and Butler, 1996; Yang and Gu, 2006).

Lim et al. (1996) used a 53-L (bulk volume) sand-pack model to study solvent-assisted gravity drainage for Cold Lake heavy oil. Butler's SAGD equation was used to determine the diffusion coefficient and the peak oil production rate when the solvent chamber reached the top of the reservoir model. The effective diffusion values determined for ethane and propane were 100 times greater than molecular diffusion. As a result, Lim et al. (1996) pointed out that mechanical dispersion was the most likely process for bitumen recovery in solvent-assisted gravity drainage.

Khalifi et al. (2020) developed an experimental setup to measure the diffusivity of dimethyl ether into heavy oil to quantify the molecular diffusion coefficient. They conducted the experiment in a closed PVT system at possible SAGD conditions, and concluded that a greater concentration effect would be expected in molecular diffusion if a heavier oil was considered.

Das (2005) used reservoir simulation for the history-matching of VAPEX using propane. The size of the field-scale 2-D section simulation model was 20 m by 60 m. The grid block size used in the simulation was 0.4 m in all directions in an attempt to control the numeral dispersion. He studied the mixing between injected solvent and bitumen for some cases using dispersion coefficients. Very large dispersion coefficients in the order of $10^{-2}$ $cm^2$/s or $8.64 \times 10^{-2}$ $m^2$/day were needed to match production rates for all cases.

There is a lack of dispersion coefficient data for mixtures of solvents and bitumen under gravity drainage. This research provides a new set of experimental data for the mixing of solvent and bitumen under gravity drainage and reports the dispersion coefficients resulting from the history matching of the experimental data. The experimental program verified in this research offers a way to systematically compare different solvents for SA-SAGD with their quantifiable dispersion coefficients under given chamber conditions.

## 2. Small scale gravity experiment

The experiments were designed to investigate the effects of the chamber conditions (pressure, temperature, and solvent/steam composition) on oil recovery under gravity drainage. The important points in the investigation included:

- Bitumen drainage rate and recovery factor.
- Condensation of solvent and water and the subsequent mixing of solvent with bitumen.
- Properties of the produced bitumen.

This is a new type of gravity drainage experiment that is relatively simple and easy to set the thermodynamic conditions. It allows for a comparative study of different solvents for co-injection in a relatively short time frame. The drainage of one experiment takes a few hours

compared to a few days of the large-scale experiments as presented in Sheng et al. (2021b).

Three experiments were performed to verify this new experimental program: SAGD, $C_8$-SAGD with 10 mol% $nC_8$, and $C_4$-SAGD with 20 mol % $nC_4$. Since $C_8$-SAGD was expected to perform better than $C_4$-SAGD, the concentration of $nC_4$ in $C_4$-SAGD was set to be a larger value than that of $nC_8$ in $C_8$-SAGD. The pressure used in the small-scale experiment was 3500 kPa based on one of the thermal bitumen production projects in Alberta, Canada. Besides thermodynamic conditions, however, petrophysical properties of the sand-pack were designed to ensure the thermal effect did not dominate the dilution (or mixing) effect on oil viscosity reduction. Therefore, the sand-packs used were much more permeable than typical bitumen reservoirs as will be given later; it is not the objective of the experiment to mimic petrophysical properties of any actual reservoirs or to mimic the transient flow regime of field-scale SA-SAGD.

### 2.1. Experimental setup

Fig. 1 shows a schematic of the experimental setup. The main component of the experiment was a 25-L steel cylindrical vessel of 24 inches in length and 4.5 inches in outer diameter as shown in Fig. 2. It accommodated a sand-pack of 15 inches in length and 3 inches in diameter. The sand-pack was placed at the upper portion of the steel vessel attached to the vessel lid and held in place by a thin steel mesh. The lower portion of the vessel was a liquid collection container that was about 8 inches in height. There was also about one inch of void annular space between the sand-pack and the inner wall of the steel vessel.

Inside the vessel, there were an injector, a top producer, and a bottom producer. With just one opening, the injector was inserted into the void space towards the top of the liquid collection container. The injector opening was oriented towards the inner wall of the vessel, away from the sand-pack. The top producer was connected to the outlet line and used to produce excess vapor. The bottom producer consisted of the liquid collection container and the liquid drainage line. The produced oil-water emulsion was first drained from the sand-pack into the liquid collection container and pumped out of the vessel via a liquid drainage line.

There were two fluid lines connected to the top lid of the vessel. The first line was the inlet line, one end of which was connected to the injector. The upstream of the inlet line was connected to a steam generator and injection pump. The second line was the outlet line, one end of which was connected to the top vapor producer. The downstream of the outlet line was connected to a pressure control valve, a coil tubing condenser, and a wet test meter. The pressure valve was used to maintain pressure by regulating any excess vapor inside the vessel. Any excess vapor was measured by a wet test meter and collected with cylinders or production tanks.

There were also four thermocouple lines used to monitor the temperatures inside the vessel. Three thermocouple lines were placed inside the sand-pack, with one in the middle and two on the side of the sand-pack. The fourth thermocouple line was inserted into the annular void space. Each thermocouple line contained five thermocouple reading points, providing a total of 20 temperature reading points inside the vessel, with 15 points inside the sand-pack. The steel vessel was covered by three band heaters to control heat losses from the vessel.

Below is a list of the equipment pieces used along with more detailed specifications (Fig. 1):

- Isco 500D and Isco 1000D syringe pumps with the maximum operating pressure of 34.0 MPa.
- One steam generator with a power rating of 15 kW at 480 V.
- One flow control air-actuated valve controlled by a digital-to-analog system.
- Five band heaters with two top heaters with 360 W at 208 V and three bottom heaters with 2.0 kW at 208 V.
- A stainless-steel condenser connected to a glycol chiller.
- A drum-type gas meter with a maximum flow rate of 900 L/h.
- Four sets of multi-point (five reading points on each set) thermocouples.

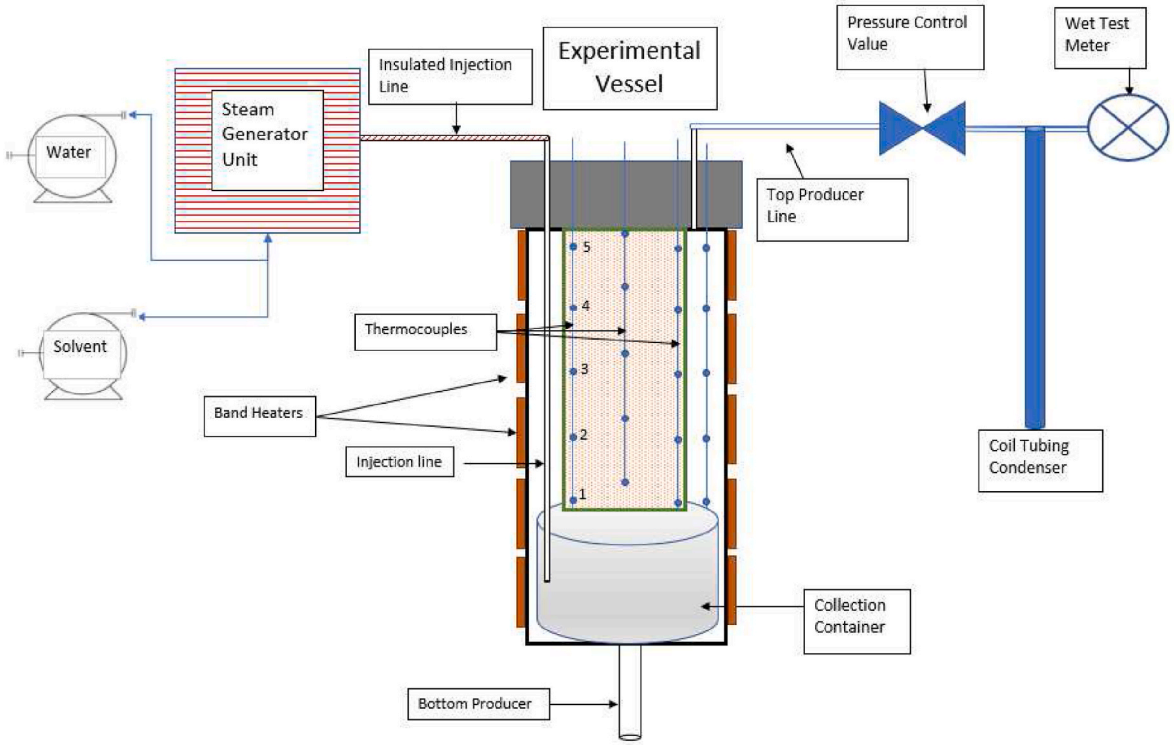


**Fig. 1.** Schematic of the experimental setup in this research. Steam and solvent are co-injected into the void space of the vessel and not directly into the sand-pack. The top producer line produces any excess injected vapor. The bottom producer collected the produced oil-water emulsion.

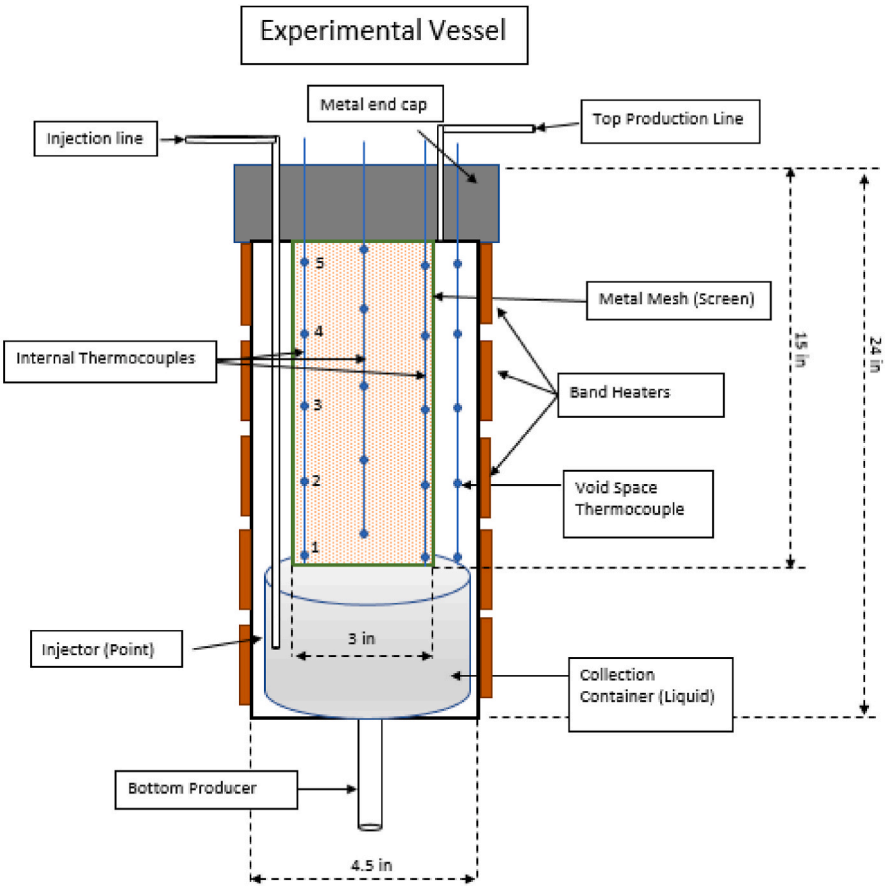


a) Side view of the experimental vessel

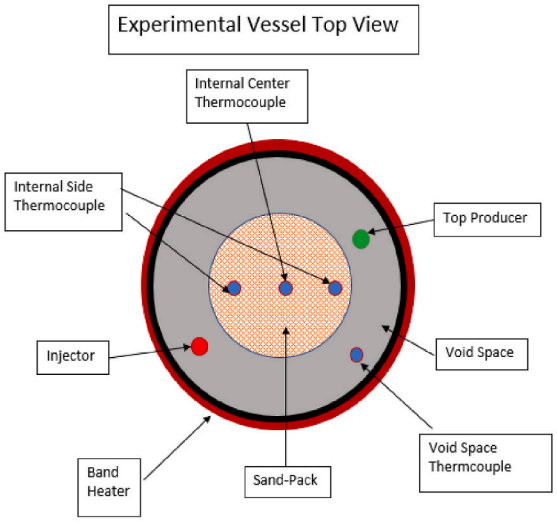


b) Top view of the experimental vessel

**Fig. 2.** Schematic of the experimental vessel and its components inside. The main steel vessel houses the sand-pack and four sets of thermocouples with 20 temperature reading points in total. Three sets of thermocouples are inserted into the sand-pack, and one set of the thermocouples is inserted into the annular space.

Three experiments were conducted, one SAGD and two SA-SAGD experiments with the following solvents: $nC_8$ at 10 mol% and $nC_4$ at 20 mol%. The pressure of the vessel was controlled at 3500 kPa after pressure ramp up, and the temperature of the injected vapor phase ranged from 229 °C to 241 °C depending on the composition of the injection vapor. These saturation temperatures for SA-SAGD were determined by using the Peng-Robinson equation of state (PR EOS) as presented in Venkatramani (2014) and Venkatramani and Okuno, 2018a, 2018b for n-alkanes/water binary mixtures.

The experiment was designed not to inject the fluid directly into the sand-pack but to let the injected gaseous phase saturate the void space. The thermal and compositional mechanisms mobilized the oil, and then

the oil was drained under gravity. The injection rate for all experiments was set to 3987 $cm^3$/min at in-situ conditions (3500 kPa and saturation temperature for each experiment). This rate corresponds to 70 $cm^3$/min (cold-water equivalent, CWE) of steam for SAGD at the pump conditions (101 kPa, 22 °C). SA-SAGD injection rates at pump conditions were then calculated from the determined in-situ rate of 3987 $cm^3$/min. This injection rate was to control the composition and, therefore, the temperature in the void annular space for SA-SAGD cases. Through numerical simulations and trial experiments, we confirmed that all SA-SAGD experiments would have a steady composition in the void space with this in-situ rate. The SAGD experiment was first performed and served as the baseline for the subsequent SA-SAGD experiments. This way, one can compare the effectiveness of adding solvent in bitumen recovery.

### 2.2. Oil properties

The bitumen used in the experiments was from northern Alberta. Details of the experimental data and procedures for the fluid modeling were described in Sheng (Gao et al., 2017) (not duplicated here). It had a molecular weight of 560 g/mol with a density of 1015.24 kg/$m^3$ at 15 °C and 101.3 kPa. Table 1 shows the compositions and SARA analysis of the bitumen. Densities, viscosities, and saturation points of three bitumen/solvent mixtures were measured over a wide range of conditions, up to 200 °C and 10,000 kPa. Table 2 gives the bitumen sample viscosity and density data at various temperatures. The bitumen was split into two pseudo-components, B1, and B2, for EOS modeling. The PR EOS model was calibrated by matching PVT test data. Kumar and Okuno's method (Kumar and Okuno, 2016) was used for vapor pressure properties, such as Tc, Pc, and ω, for B1 and B2 pseudo-components and binary interaction parameters (BIPs) between bitumen and solvent components. Tables 3 and 4 summarize the component properties, molecular weights, and BIPs. Viscosity and density models were also developed for the bitumen by matching experimental data. The calibrated EOS, density, and viscosity models of bitumen and solvent accurately represented the experimental data, and they were used in SAGD and SA-SAGD simulations (section 3).

### 2.3. Model packing and oil saturation

The sand-pack had a diameter of 3 inches and a height of 15 inches. It was packed into a thin steel mesh sleeve and then inserted into a core holder. The sand-pack consisted of unconsolidated quartz sand and had a bulk volume of approximately 1700 $cm^3$, with about 570 $cm^3$ of the pore volume. Fig. 3 gives the grain size distribution of sand grains used for the sand-pack. Deionized water at room temperature (22 °C) was used to saturate the sand-pack and also used to measure the porosity and permeability, 0.33 and 76 D, respectively. Then, the heated bitumen at 70 °C was injected into the sand-pack, displacing the water. Initial water saturation ranged from 7.2% to 8.7%. Different sand-packs had slightly different pore volumes and initial saturations of water and oil (Table 5). Once the sand-pack was saturated with bitumen and water, it was transferred to the experimental steel vessel and sealed with the top lid.

The experiments in the current research were designed to avoid complicated flow regimes induced by strong capillary forces in the imbibition of a wetting phase, by considering the results of Sheng et al. (2021a, b). Therefore, the sand-pack in this research was designed to simplify and reduce the impact of capillary forces during the experiment by using the grain size distribution shown in Fig. 3. It was purposefully made by using only a few large mesh sizes.

**Table 1**
SARA analysis for the bitumen sample used in this research.

| | Weight % |
|---|---|
| Asphaltenes | 18 |
| Saturates | 19 |
| Aromatics | 39 |
| Resins | 18 |
| Recovered | 94 |
| Unrecovered | 6 |

**Table 2**
Bitumen (dead oil) densities and viscosities at different temperatures at 101 kPa.

| Properties | Values |
|---|---|
| Density at 15 °C, kg/$m^3$ | 1015.24 |
| Density at 40 °C, kg/$m^3$ | 999.42 |
| Density at 80 °C, kg/$m^3$ | 974.10 |
| Viscosity at 15 °C, cp | 1,000,000 |
| Viscosity at 40 °C, cp | 24,000 |
| Viscosity at 80 °C, cp | 675 |

**Table 3**
Parameters for the two-component bitumen model using the PR EOS. The EOS model was calibrated with experimental data by use of the method of Kumar and Okuno (2016).

| | Mol % | MW, g/mol | Tc, °C | Pc, kPa | Acentric factor |
|---|---|---|---|---|---|
| B1 | 49.5 | 283.0 | 526.35 | 2000 | 0.3996 |
| B2 | 50.5 | 831.1 | 976.62 | 1314 | 0.8712 |

**Table 4**
BIP values used for the 2-component bitumen model using the PR EOS. All other BIPs are zero. Kumar and Okuno's correlations (Kumar and Okuno, 2016) were used.

| | $nC_4$ |
|---|---|
| $nC_4$ | 0 |
| $nC_8$ | 0.0337 |
| B1 | 0.0625 |
| B2 | 0.0795 |

### 2.4. SAGD experiment

Table 6 shows the temperature and rate of steam injection. Before the start of each experiment, the air in the void space of the vessel was purged with nitrogen gas. The nitrogen gas was then produced along with the injected steam through the top producer. Subsequently, the preheating of the entire vessel was performed by using the band heaters attached to the outside of the vessel wall. The band heaters were turned on to the maximum power for 5 min, increasing the temperature readings in the void space to 70 °C, and the sand pack temperatures to 30–35 °C. The cumulative energy input from the band heaters during the entire experiment was approximately 2.9 kWh as shown in Fig. 4. The initial energy output from the band heaters minimized the condensation during the initial steam injection while ensuring bitumen was not mobilized by heating from the band heaters. After preheating, the band heaters were set to 5 °C above the saturation temperature to limit the heat losses from the vessel. The steam was injected at a constant rate of 70 $cm^3$/min CWE at 3500 kPa and 241 °C. The pressure was ramped up at a rate of 200 kPa per minute until the vessel reached the target pressure of 3500 kPa. The back-pressure regulator was opened on the top producer line to regulate the vessel's pressure and ensured a steady pressurization rate. It controlled the pressure in the vessel afterward to maintain the target pressure of 3500 kPa. Any condensation that occurred during this time was captured by the bottom collection container.

The first batch of the condensed liquid was drained by the bottom producer right after the pressure reached 3500 kPa. Produced liquids in the collection container were drained with an interval ranging from 22

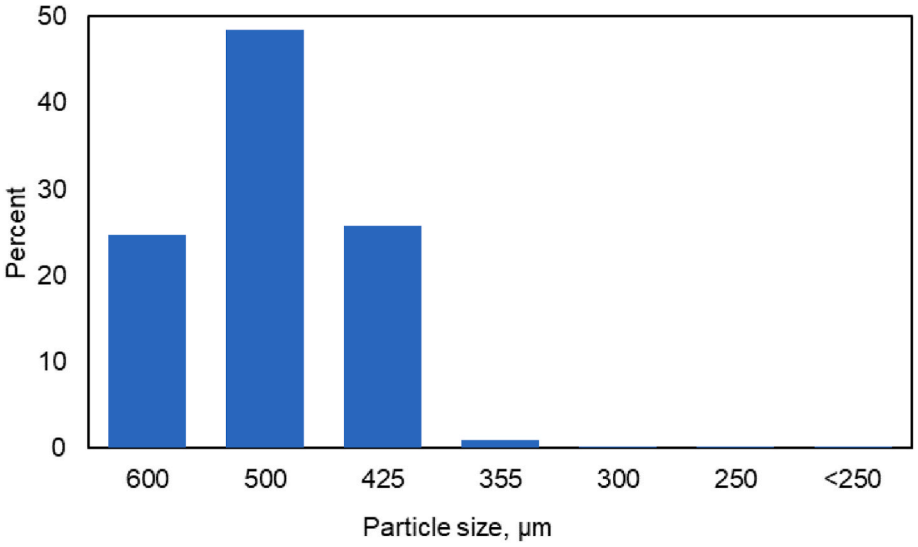


**Fig. 3.** Grain size distribution of the sand-pack with an average grain size of 500 μm.

**Table 5**
Sand-pack pore volumes and initial saturations for the SAGD and SA-SAGD experiments.

| | Pore volume, $cm^3$ | Oil saturation, % | Water saturation, % | OOIP, $cm^3$ |
|---|---|---|---|---|
| SAGD | 519.13 | 92.85 | 7.15 | 482.03 |
| $C_8$-SAGD | 531.93 | 91.68 | 8.32 | 487.69 |
| $C_4$-SAGD | 524.74 | 91.89 | 8.11 | 482.2 |

**Table 6**
Injection rates and saturation temperatures for SAGD and SA-SAGD experiments. The pump conditions for steam were 22 °C and 3500 kPa, while the pump conditions for solvent were 7 °C and 2500 kPa.

| | Temperature, °C | Steam rate at pump condition (CWE), $cm^3$/min | Solvent rate at pump condition, $cm^3$/min | Total in-situ condition rate, $cm^3$/min |
|---|---|---|---|---|
| SAGD | 241 | 70 | 0.00 | 3987 |
| $C_8$-SAGD 10 mol% | 236 | 61.86 | 62.03 | 3987 |
| $C_4$-SAGD 20 mol% | 229 | 54.06 | 72.93 | 3987 |

to 35 min in the first 2 h, and approximately every 1 h afterward. During a single drainage period, the drainage valve on the bottom producer line was turned on and off multiple times until all fluid accumulated was collected. Typically, the drainage period lasted for 5–10 min and was reflected by a momentary pressure drop in the steel vessel system.

After the last drainage period, the fluid injection was stopped, the band heaters were turned off, and the vessel system was cooled and depressurized. The entire SAGD test lasted for 5 h in total. Finally, the model was dismantled. The sand-pack was extracted, excavated, and divided into three segments: top, middle, and bottom of the model. A sample of the sand-pack from each segment was taken for each experiment and was subjected to asphaltene and oil/water/solid analysis. The produced liquids were also measured for carbon number (CN) distribution, density, viscosity, molecular weight, and asphaltene mass concentration in the produced oil.

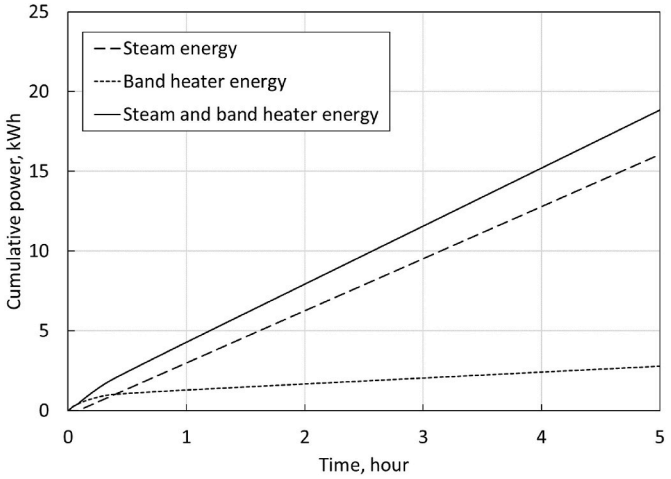


**Fig. 4.** Cumulative power input from the band heater and the injected steam for SAGD. The band heater only added a limited amount of power to the system after 20 min of steam injection.

### 2.5. SA-SAGD experiments

Table 6 shows the temperature and rate of steam-solvent coinjection. The experimental procedure for SA-SAGD was similar to that of SAGD, except in three main points. Firstly, the solvent ($C_8$ or $C_4$) was co-injected with water at 3500 kPa and 7 °C into the steam generator, at which the solvents were in a liquid state. The steam generator then heated the injection fluid to the corresponding saturation temperature at 3500 kPa (236 °C for $C_8$-SAGD and 229 °C for $C_4$-SAGD) and injected it into the experiment vessel through the inlet line.

Secondly, the band heaters were set 5 °C above the injection saturation temperature, which varied for different experiments because of their different compositions. Thirdly, liquid drainage at the bottom producer was performed more frequently for SA-SAGD compared to SAGD because the SA-SAGD experiments resulted in more rapid oil production. Therefore, liquid drainage was conducted with an interval between 9 and 21 min for the first 2 h, and approximately every 30 min afterward.

For the $C_4$-SAGD case, the produced solvent from the top of the vessel

(gaseous stream) was collected in large production tanks. Then, these production tanks were depleted while connected to a wet test meter to measure the amount of $C_4$ produced. The liquid stream from the bottom of the vessel during sampling was collected, and the solvent separated from the produced oil was directed to a wet test meter to measure the volume of $C_4$ produced.

For the $C_8$-SAGD case, the produced solvent from the top of the vessel was directed into a condenser to collect liquid water and any produced heavy ends in graduated cylinders. Then, the stream was connected to a wet test meter to measure the volume of the produced gaseous solvent. The liquid stream collected from the bottom of the vessel during sampling was collected into graduated cylinders.

The oil samples collected from the bottom of the vessel were then processed to determine the amount of water and solvent in the mixture. The water was separated first by adding toluene, and then the solvent in oil is determined using rotary evaporation.

### 2.6. Experimental results

Fig. 5 shows the pressure data for both SAGD and SA-SAGD experiments. The pressures in the ramp-up phase were similar between the three experiments. The target pressure of 3500 kPa was achieved no later than 20 min after the commencement of injection. Pressure drops of up to 500 kPa after reaching the target pressure indicated the time of liquid drainage.

Fig. 6 shows the histories of hydrocarbon production rates. In all three experiments, the oil rate (Fig. 6a) peaked within the first half-hour of injection, and then leveled off after 1.5 h. The peak rate was 9.8 $cm^3$/min with SAGD, 14.6 $cm^3$/min with $C_4$-SAGD, and 31.3 $cm^3$/min with $C_8$-SAGD. The oil rate in the $C_8$-SAGD experiment declined most rapidly. In contrast, the oil rate of SAGD declined most slowly. Fig. 6b shows the $C_4$ production rate from the bottom producer at standard conditions. The production history of $C_4$ from the top producer was not measured to avoid safety issues of the storage tank; therefore, it is not reported here. Fig. 6c shows the $C_8$ production rate from both the bottom and top producers at standard conditions. The first peak in the two figures appeared approximately at 0.5 h, when the oil recovery rate was the highest. The subsequent peaks appeared when oil was almost depleted; that is, the solvent components had accumulated at the bottom of the vessel. The cumulative injection and production history of solvents will be shown later for discussion of simulation results.

Fig. 7 and Table 7 show oil production data for the three

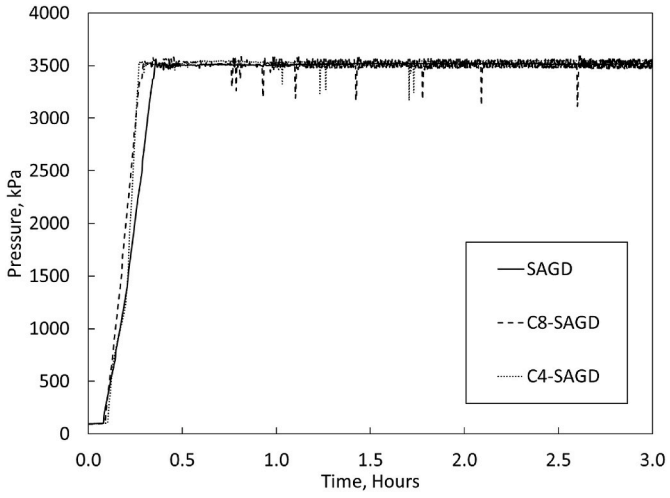


**Fig. 5.** The pressure inside the vessel for SAGD and SA-SAGD experiments. After the temperature reached the target saturation temperature, the pressure was held constant at 3500 kPa. Pressure dips afterward indicate when fluid drainage was done from the bottom producer.

experiments. Since OOIPs were slightly different for all experiments, the oil recovery factor (i.e., the ratio of the total produced oil to the OOIP) was used to compare the experimental results. The total recovery factors for SAGD, $C_4$-SAGD, and $C_8$-SAGD were 78%, 84%, and 89%, respectively; that is, $C_8$-SAGD had the highest total recovery factor, followed by $C_4$-SAGD and SAGD. Compared to SAGD, the addition of solvent in SA-SAGD increased bitumen mobilization and decreased the remaining oil. Although the solvent molar concentration for $C_4$-SAGD was two times greater than that for $C_8$-SAGD, the clear difference in oil production between the two solvents demonstrates the importance of solvent volatility and dilution capability in SA-SAGD.

The second and third oil recovery data points in $C_8$-SAGD had unexpectedly high water cuts (99% and 75%, respectively), followed by the fourth data point with a high oil cut (80%). It appeared that the produced bitumen had not been fully recovered from the second and third drainage of the bottom producer and, therefore, the remaining oil was recovered in the subsequent drainage stages. The history matching process for $C_8$-SAGD relied more on temperature data than the second and third oil recovery data points.

Fig. 8 shows the temperature histories of the void space and central sand-pack thermocouples for the three experiments. The void space temperature increased rapidly after injection, while the temperature inside the sand-pack increased more slowly. The temperature change in the void space was also directly related to the pressure change in the system. The void space temperature profiles for all cases were similar. The temperature inside the void space after the transient period matched with the injection temperature, which indicated that the composition of the injection fluid was steady and that the designed saturation temperatures were successfully obtained.

Inside the sand-pack, the temperature at the top thermocouple was higher than that at the lower thermocouples. In addition, the temperature increase at the top thermocouple was more rapid than that at the lower thermocouples. The temperature of the sand-pack for SAGD and $C_4$-SAGD increased smoothly in the transient period.

As for $C_8$-SAGD, the internal temperature increased gradually and then drastically at a particular time. This event indicated the arrival of the steam (vapor) front at this location. The temperature data (Fig. 8b) at different thermocouple locations confirmed with a high degree of confidence the advancement of the steam front from top to bottom. The thermocouple data supported the observation that $C_8$-SAGD produced oil much faster than SAGD and $C_4$-SAGD.

The produced oil samples were analyzed for density and carbon number distribution. The produced oil density for SAGD, $C_8$-SAGD, and $C_4$-SAGD were 1020.30 kg/$m^3$, 1021.40 kg/$m^3$, and 1022.23 kg/$m^3$ (at 15 °C), respectively. They deviated slightly from the original bitumen density, 1015 kg/$m^3$.

Fig. 9 shows the carbon number distribution data for the produced bitumen samples. Only the recoverable fraction was reported in this figure. The recovery factors of the oil samples in SAGD, $C_4$-SAGD, and $C_8$-SAGD were 47, 42, and 56 wt%, respectively. The weight percentage of light components (CN < 20) in the produced oil sample for SAGD was greater than that for $C_8$-SAGD and $C_4$-SAGD. The weight percentage of heavy components (20 < CN < 60) in the produced oil for SAGD was lower than that for $C_8$-SAGD and $C_4$-SAGD. Beyond a CN of 60, the weight percentage distributions were similar among all cases. This observation indicates that the solvent was able to mobilize heavier components in the bitumen compared to SAGD.

After the experiment, Dean-Stark and asphaltene analysis were performed on the excavated sand-pack, with the results summarized in Table 8. The remaining oil saturation in the sand-pack was smaller in $C_8$-SAGD than in $C_4$-SAGD and SAGD. This reflects the greater total oil recovery factor observed for $C_8$-SAGD.

Furthermore, for all cases, the bottom of the sand-pack contained the highest water saturation compared to the middle and the top of the sand-pack because of the capillary/gravity equilibrium. For all experiments, the oil saturation increased from the top to the bottom of the sand-pack

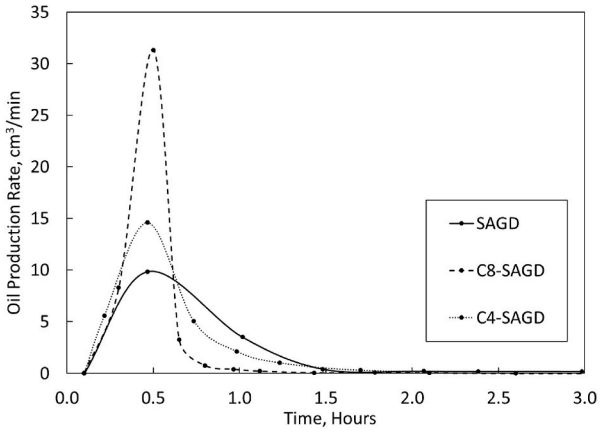


(a) Total bitumen production rate

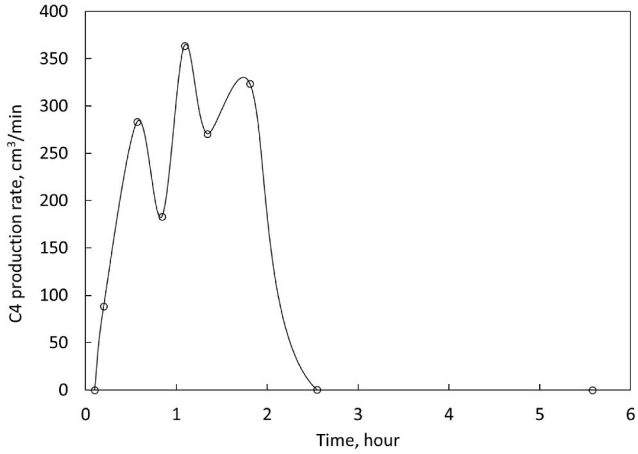


(b) $C_4$ production rate from the bottom producer at standard conditions. The production history of $C_4$ from the top producer was not measured, and therefore not shown here.

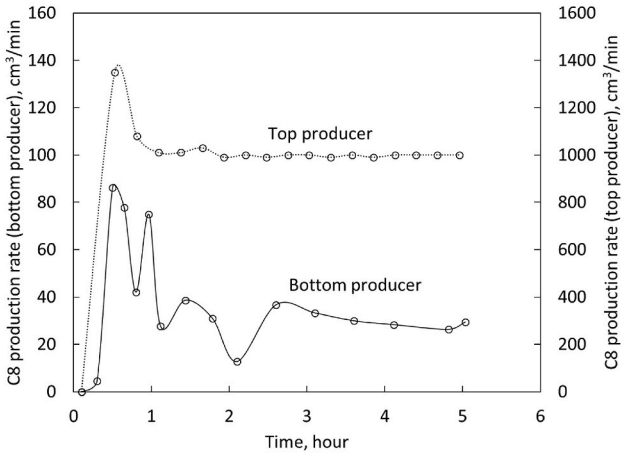


(c) $C_8$ production rate from the bottom and top producers at standard conditions.

**Fig. 6.** Bitumen and solvents production rates of SAGD and SA-SAGD experiments. The fluid production started soon after the preheating period, 0.1 h.

because the top of the sand-pack contained more steam, and the bottom contained more hot water. Thus, the oil saturation in the vapor zone was residual to steam, which should be smaller than the oil saturation after being displaced by only hot water.

Asphaltene weight percentage in the remaining oil for SAGD and $C_4$-SAGD ranged from 20 to 26%, slightly higher than 17% in the original bitumen. In sharp contrast, the remaining oil for $C_8$-SAGD contained 40–70% asphaltene by weight. Note, however, that the remaining oil saturation for $C_8$-SAGD was 4–10 times smaller than those for the other cases.

Fig. 10 shows the photos of the excavated samples for SAGD, $C_4$-SAGD, and $C_8$-SAGD. The color of the samples gradually changed from dark to light in the direction from the bottom to the top of the sand-pack for each case. The SAGD sample photo shows the darkest color throughout the sand-pack, while the sample colors for $C_4$-SAGD are slightly lighter. The ones for $C_8$-SAGD are the lightest in color, with the

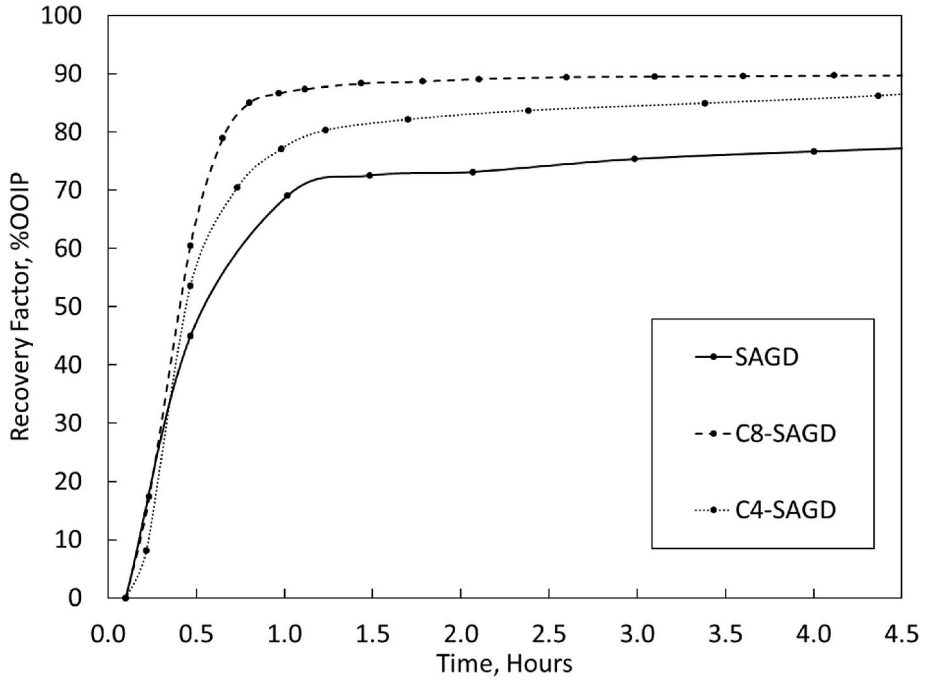


**Fig. 7.** Recovery factors of SAGD and SA-SAGD experiments. Total recovery factors for $C_8$-SAGD, $C_4$-SAGD, and SAGD are 89%, 84%, and 78%, respectively.

**Table 7**
Total oil production and production duration of SAGD and SA-SAGD along with recovery factor at 1 h and ultimate recovery factor.

| | Total oil produced, $cm^3$ | Total oil recovery factor | Recovery factor at 1 h | Time to total recovery, hours |
|---|---|---|---|---|
| SAGD | 375.44 | 78% | 71% | 5.05 |
| $C_8$-SAGD | 406.49 | 89% | 85% | 4.93 |
| $C_4$-SAGD | 422.05 | 84% | 80% | 4.78 |

top and the middle samples showing colors similar to that of the original sand. The excavated sample photos and the saturation analysis consistently show that SA-SAGD performed better than SAGD in terms of oil recovery, and that the $C_8$ solvent was more effective in diluting bitumen compared to $C_4$.

## 3. Simulation and history matching

### 3.1. Simulation procedure

The simulation was performed with the CMG STARS simulator (Computer Modelling Group) (Computer Modelling Group, 2018). Important inputs of the simulation model included gridblock sizes and coordinates, well placement, petrophysical properties throughout the whole physical model, fluid properties, and well and heater controls. The simulation model was assigned two sets of properties, one for the sand-pack and the other for the void space according to the setup of the physical model.

Fig. 11 shows that the simulation model used a cylindrical coordinate system in the up-right direction with the sand-pack surrounded by annular void space. In the cylindrical coordinate system, the horizontal, radial, and vertical directions are referred to as *I*, *J*, and *K*, respectively. The gridblock dimensions in the sand-pack region and the annular void space were 0.22 cm, 360°, and 0.24 cm in *I*, *J*, and *K*, respectively. The numbers of gridblocks were 22, 1, and 144 in the *I*, *J*, and K directions, respectively. Therefore, the sand-pack had 22 radial cylindrical rings layered horizontally, with a distance of 0.22 cm between the circles. The model was vertically divided into 144 gridblocks with a thickness of 0.24 cm. The gridblock dimensions of the void space under the sand-pack were 0.22 cm, 360°, and 0.3 cm in the *I*, *J*, and *K* directions, respectively. The number of gridblocks was 22 in *I*, 1 in *J*, and 56 in *K*. In total, the model consisted of 4400 gridblocks ($I = 22$, $J = 1$, and $K = 200$).

The injector was a single gridlock placed in the annular space under the sand-pack. There were two producers in the physical experiment; the top producer continuously produced gas, while the bottom producer produced only liquid. The bottom producer in the simulation is a series of gridblocks at the very bottom of the model.

The injector was set to inject the fluid at a constant pressure of 3500 kPa and the corresponding saturation temperature. The outermost gridblock of the model was set to be the band heater with steel's thermal conductivity. These gridblocks had zero porosity and permeability; hence they only allowed heat transfer with no mass transfer. The experimental band heater temperature data were imported to the simulation model as the input parameters for the band heater.

A porosity of 0.33 and a permeability of 75.7 D were used for the whole sand-pack region in the numerical model. The maximum allowed porosity of 0.999 and permeability of 999 D were set to the gridblocks in the annular void space. The initial fluid saturations were taken from the experimental data. The fluid models of bitumen and solvent used in this simulation were directly taken from the calibrated fluid models (EOS, viscosity, and density models) as described in section 2.2. K-values were generated with the EOS model using STARS' phase equilibrium calculation. The oil phase density model followed the ideal mixing law. The modified Arrhenius model within STARS was used for a flexible correlative capability for viscosities of bitumen/solvent mixtures, in which the scaling factors for bitumen/$C_4$ and bitumen/$C_8$ were based on Venkatramani and Okuno (Venkatramani, 2014; Venkatramani and Okuno, 2018a, 2018b).

The thermal conductivities of the sand-pack, water, oil, and gas

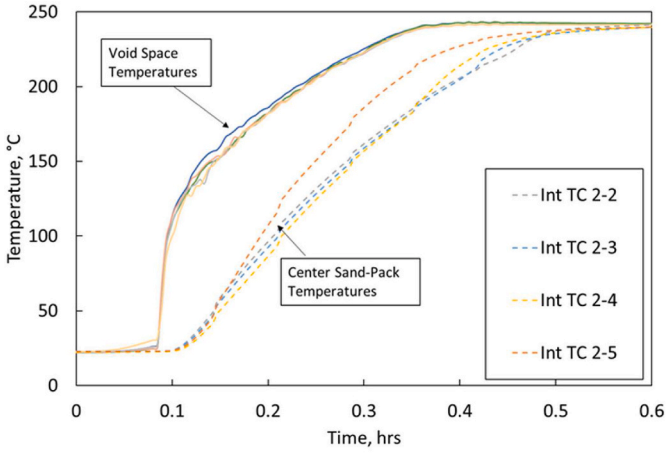


a) SAGD temperature histories.

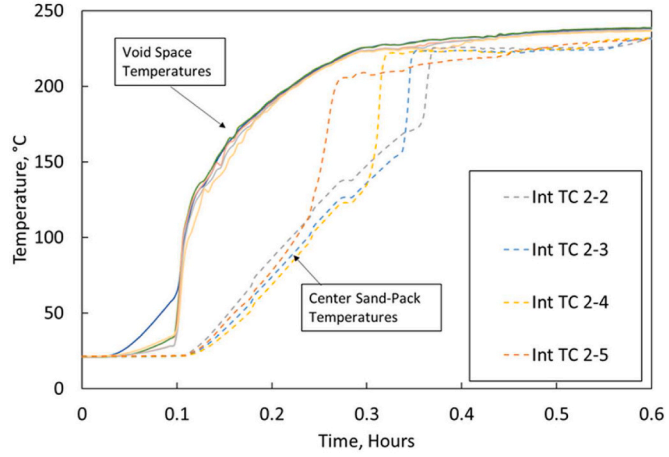


b) $C_8$-SAGD temperature histories.

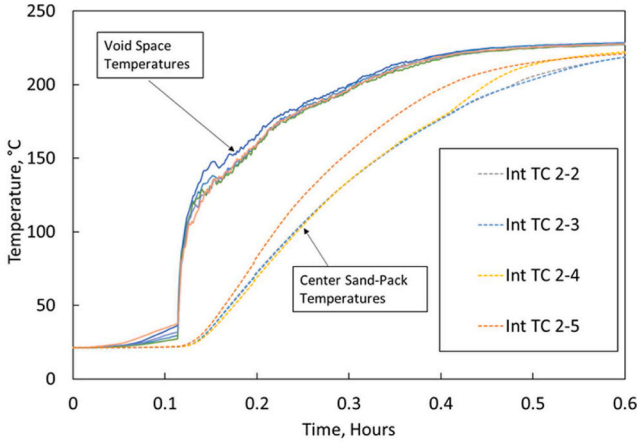


c) $C_4$-SAGD temperature profile

**Fig. 8.** Temperatures from void space thermocouples and central thermocouples inside the sand-pack ("Int TC 2-2" to "Int TC 2–5"). The solid lines represent the temperatures of the void space thermocouples, while the dotted lines represent the temperatures of the central thermocouples inside the sand-pack. Thermocouple 5 was located at the top, while thermocouple 2 was located at the bottom. Note that the sand-pack temperature profile for $C_8$-SAGD had a rapid increase at 0.3 h, detecting the steam front.

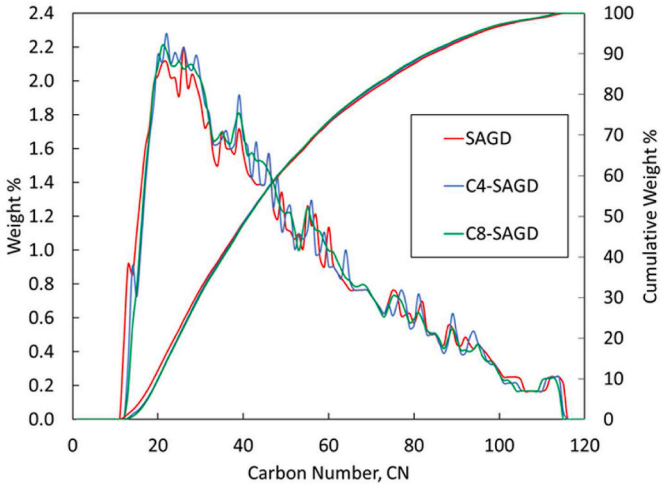


**Fig. 9.** Carbon number distribution of the produced bitumen for SAGD and SA-SAGD. This figure shows only the recoverable fraction in simulated distillation. Recovery factors for SAGD, $C_4$-SAGD, and $C_8$-SAGD cases were 47, 42, and 56 wt%, respectively.

**Table 8**
Oil/water/gas analysis for the excavated sand samples and asphaltenes content in the remaining oil for the SAGD and SA-SAGD experiments. $C_8$-SAGD had the smallest remaining oil saturation, and the highest asphaltene concentration in the remaining oil.

| Layer | Saturation % at 23 °C | | | Asphaltene wt% in oil |
|---|---|---|---|---|
| | Water | Oil | Gas | |
| a) SAGD experiment | | | | |
| Top | 1.6 | 8.6 | 89.7 | 22.8 |
| Middle | 1.7 | 13.0 | 85.3 | 23.4 |
| Bottom | 2.2 | 15.3 | 82.5 | 22.5 |
| b) $C_4$-SAGD experiment | | | | |
| Top | 1.1 | 8.1 | 90.9 | 22.0 |
| Middle | 1.1 | 10.8 | 88.1 | 24.7 |
| Bottom | 1.1 | 24.3 | 74.5 | 26.4 |
| c) $C_8$-SAGD experiment | | | | |
| Top | 2.1 | 1.6 | 96.3 | 43.3 |
| Middle | 2.6 | 0.5 | 96.9 | 73.6 |
| Bottom | 2.6 | 4.7 | 92.7 | 43.9 |

phases used in the simulations were 1.5, 0.36, 0.072, and 0.02 J/(cm × min × °C), respectively. The steel thermal conductivity of 20 J/(cm × min × °C) was used for the band heater. The formation compressibility was set to $1.21 \times 10^{-5}$ $kPa^{-1}$. It was obtained from the authors' previous research (Sheng et al., 2021a; Sheng, 2021) using the same sand, under similar temperature and pressure conditions.

Fig. 12 shows the relative permeability curves of the two phases for the sand-pack and the void space. Those curves were determined by matching the SAGD experiment results. The three-phase relative permeability calculations used Stone I correlation with the detailed parameters listed in Table 9. Residual water saturation value came from the oil imbibition process in the experiments. The residual oil saturation was determined by the oil recovery factor of the SAGD experiment.

The method for calculating the capillary pressure followed the one by Sheng et al., 2021a, 2021b. The Young-Laplace equation combined with bundles of capillary tubes indicated that the grain size distribution (Fig. 3) would result in the capillary pressure curves given in Fig. 12cd. Although it is not shown in this paper, omitting the capillary pressure affected the dispersion coefficient estimated through history-matching, and made it difficult to match the temperature distribution data.

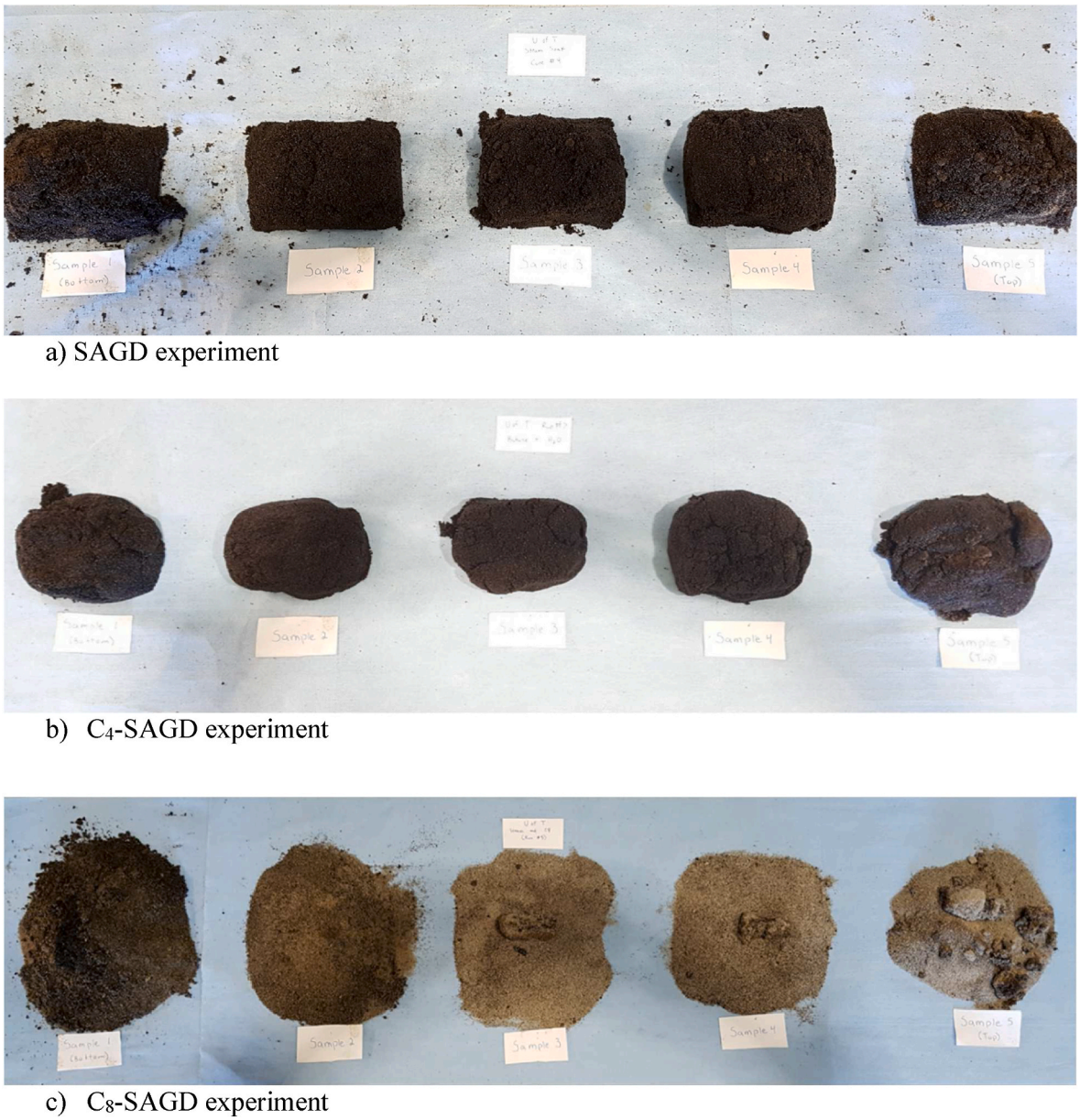


**Fig. 10.** Photos for the excavated sand samples from the SAGD and SA-SAGD experiments. Samples from left to right are from the bottom to the top of the sand-pack. The color of the sample for $C_8$-SAGD was much lighter than the other two cases (SAGD and $C_4$-SAGD) indicating higher oil recovery. (For interpretation of the references to color in this figure legend, the reader is referred to the Web version of this article.)

### *3.2. History matching of SAGD and SA-SAGD experiments*

Firstly, SAGD experimental temperature profile and oil production data were history matched. Then, the established input parameters from the SAGD history match were used for the SA-SAGD simulation model. It was important to match temperature distribution data for the SA-SAGD cases because temperature and solvent concentration were directly related to each other. Lastly, dispersion coefficients were determined to match the SA-SAGD simulation results.

Since the main mechanism of oil production in SAGD comes from viscosity reduction by temperature, the system's temperature data in the SAGD experiment were firstly matched. The matching was largely achieved by inputting the correct minute-by-minute pressure into the simulations because the system's temperature depended on the saturation pressure of the injection fluids. Then, a thermal conductivity of sand was adjusted to 1.5 J/(cm × min × °C) to improve the matching of the temperatures for the SAGD experiment. For reference, reasonable values for sand range from 1.2 to 2.0 J/(cm × min × °C). Finally, a log-linear temperature mixing rule for sand, oil, water, and gas thermal conductivity was used to better represent the temperature profile at the interface of the steam chamber. Fig. 13 shows the matching results of temperature data in the void space and the sand-pack center for the SAGD experiment. The simulated temperature profiles are in good agreement with the experimental data.

The oil production history was matched after the temperature data were matched (Fig. 14). Matching the oil production required mainly adjusting the relative permeability curve of the oil phase by reducing the exponent on the $k_{ro}$ curve from 2.0 to 1.4. As shown in Fig. 14, the final simulated oil product profile matched the experimental data of the SAGD case well.

Fig. 15 shows the oil, water, and gas saturation distributions in the history-matched simulation model at the end of the 5-h production. The capillary/gravity equilibrium with the end effect was observed in the simulation, in which higher water saturations were distributed towards

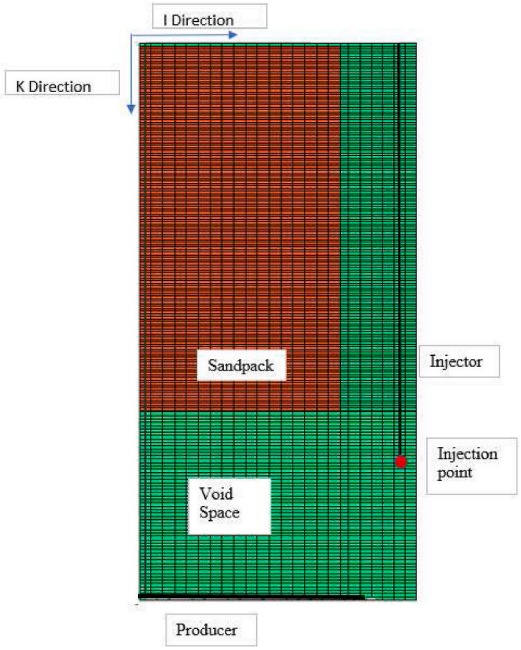


a) 2-D vertical section of the simulation model. Only half of the symmetrical model is shown.

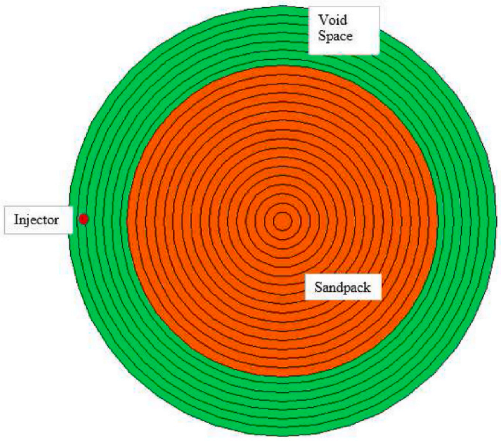


b) 2D top planar view of the simulation model.

**Fig. 11.** Sand-pack model and thermal rock types used for numerical simulation.

the bottom of the sand pack. The remaining oil saturation in the simulation model was also lower in the areas saturated by steam compared to that in the regions saturated. The oil/water/gas analysis of the excavated samples of the sand-pack also supported these observations.

The effect of solvent on temperature distributions was important for the SA-SAGD cases, especially for $C_4$-SAGD. Temperature data for the $C_8$-SAGD case were matched well with a single set of K-value tables based on the calibrated PR EOS with a given overall composition. However, matching temperature data for the $C_4$-SAGD case required modified K-value tables since using a single overall composition could not represent the significant change in composition from the void space to the sand-pack. The complexity of the phase behavior in $C_4$-SAGD has been known in the literature (Gao et al., 2017; Sheng, 2016). Therefore, the K-values were modified by a factor of 1/6 at 10 °C and 1/3 at 180 °C, which reduced the simulated solvent accumulation in the void space. Such a multiplier to K values can be viewed as a practical way to consider the compositional dependency of K values.

Once temperature data were matched, matching oil production data for the SA-SAGD cases required adjusting the dispersion coefficient of the solvent while keeping the thermal conductivity and relative permeability curves from SAGD. This allowed us to compare $C_4$-SAGD and $C_8$-SAGD with quantifiable levels of dispersion. The temperature and oil matching results are shown in Figs. 16 and 17, Figs. 18 and 19, respectively. Figs. 18a and 19a show the predicted oil production after history matching with the final dispersion coefficient values of 0.644 $cm^2$/min for $C_8$-SAGD and 0.084 $cm^2$/min for $C_4$-SAGD. Figs. 18b and 19b show the injection and production histories of $C_8$ and $C_4$ from the experiment and simulation with the above parameters. The cumulative injection and production of $C_8$ at the end of the experiment were 113.2 and 112.8 mol, respectively, and those values for $C_4$ were 219.7 and 222.8 mol, respectively. The simulation reasonably matched the experimental data in terms of solvent material balances. Note that the continuous production history of $C_4$ was not measured as previously discussed; however, the ultimate $C_4$ production value was estimated after the experiment, and we estimated an experimental material balance error that the $C_4$ production was 1.4% greater than the $C_4$ injection.

Similar to the SAGD case, the SA-SAGD cases gave the capillary/gravity equilibrium with the capillary end-effect, resulting in higher

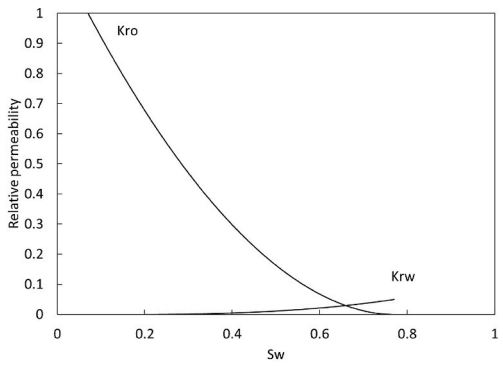


a) oil/water relative permeabilities

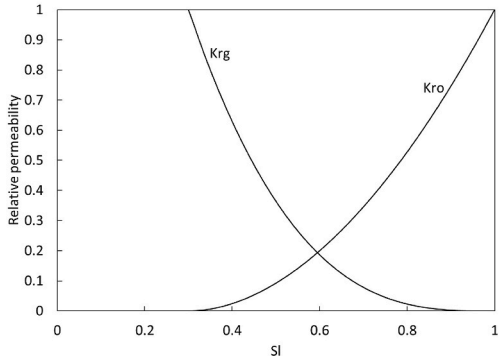


b) gas/liquid relative permeabilities

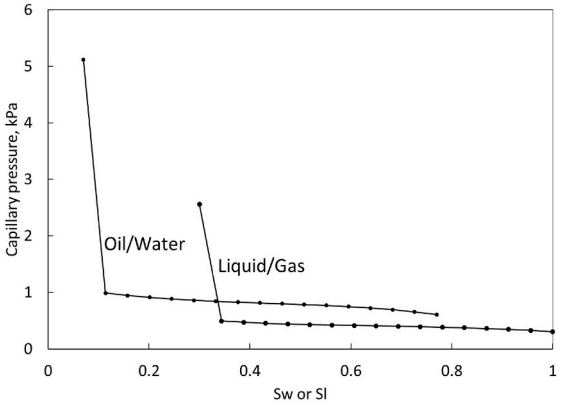


c) Capillary pressure curves for SAGD

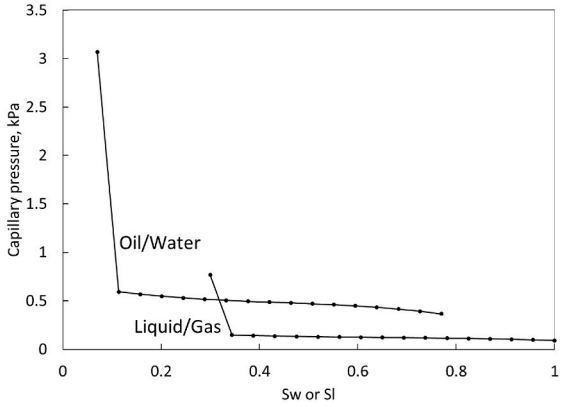


d) Capillary pressure curves for SA-SAGD

**Fig. 12.** Relative permeability curves and capillary pressure curves used for the SAGD and SA-SAGD simulations.

**Table 9**
Stone I relative permeability parameters.

| Parameter | Value |
|---|---|
| Swr | 0.7 |
| Sor (oil/water, oil/gas) | 0.23 |
| Sgr | 0 |
| Kro (Sw = Swr) | 1 |
| Krw (Sw = 1 − Sor) | 0.05 |
| Krg (Sl = 1 − Sgr) | 1 |
| Exponent, Krw | 3.0 |
| Exponent, Kro | 1.9 |
| Exponent, Krg | 3.0 |

(hot) water saturations towards the bottom of the sand-pack (Figs. 20 and 21). This was consistent with the observation from the oil/water/gas analysis for the excavated sand samples. The increase in oil recovery by SA-SAGD in comparison to SAGD depended mainly on the solvent used. That is, $C_8$ was able to dilute bitumen more effectively than $C_4$ in this research. As shown in Fig. 20, the segregation of the oil and water phases was unclear for the $C_8$-SAGD case since the diluted oil had similar densities to the water phase.

The produced oil from the simulation was split into its components B1 and B2. Fig. 22 shows that much of the incremental oil recovery by $C_8$-SAGD came from the heavier component, B2. The lighter component, B1, contributed marginally to the incremental oil recovery by $C_8$-SAGD since B1 could be recovered also by SAGD. As for $C_4$-SAGD, the incremental oil production compared to SAGD came from a small additional recovery of both B1 and B2. As a result, $C_8$-SAGD has the highest oil recovery, followed by $C_4$-SAGD and then by SAGD.

## 4. Discussion

The experimental data have indicated that different solvents result in different oil recovery results because they have different condensation and mixing characteristics. This section discusses the oil/solvent mixing characteristics obtained from the experimental and numerical results.

The convection-dispersion (CD) equation for one-dimensional and single-phase incompressible flow with a uniform porosity system is written as follows (Shrivastava, 2003):

$$-u\frac{\partial C}{\partial z}+\varphi D\frac{\partial^2 C}{\partial z^2}=\varphi\frac{\partial C}{\partial t} \tag{1}$$

where C is the mass concentration of solvent, u is the Darcy flow velocity, $\varphi$ is the porosity of the porous media, and D is the mechanical dispersion or dispersion coefficient of solvent. In the simulation, D is the input parameter measured conventionally in the lab by fitting the solution of the CD equation to the effluent concentration from a coreflood test. Therefore, it is sometimes referred to as the input dispersion coefficient.

Solving the CD equation (1) numerically using a finite-difference technique (as in the previous section) introduces numerical dispersion. The summation of the input and numerical dispersion is the simulated dispersion coefficient. Thus, equation (1) becomes (Shrivastava, 2003):

$$-u\frac{\partial C}{\partial z}+\varphi\left(D_{input}+D_{num}\right)\frac{\partial^2 C}{\partial z^2}=\varphi\frac{\partial C}{\partial t} \tag{2}$$

$$D_{input}=\frac{D_o}{\tau}+\alpha\frac{u}{\varphi} \tag{3}$$

where $D_o$ is molecular diffusion, and $\tau$ is the tortuosity of the porous

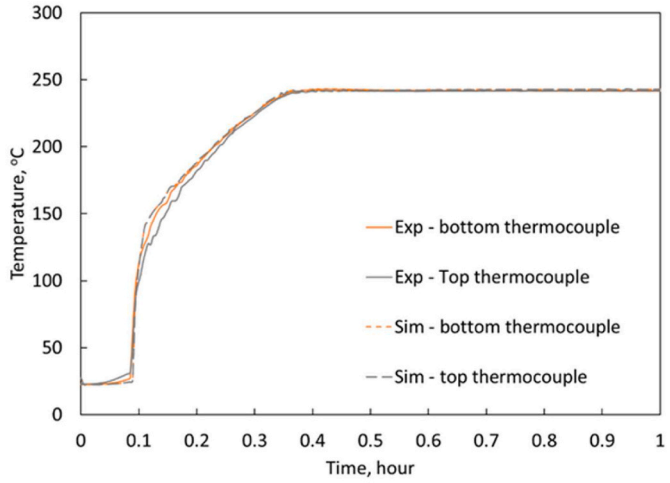


a) Temperature in the annular void space

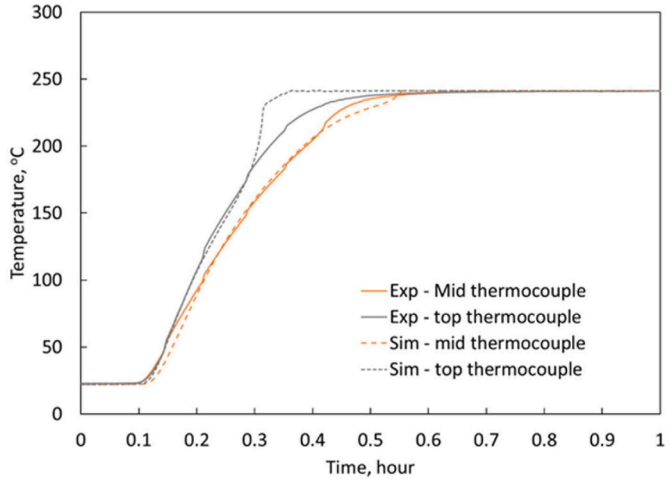


b) Central temperature of the sand-pack

**Fig. 13.** Comparison of the SAGD temperature histories from the experiment and the simulation.

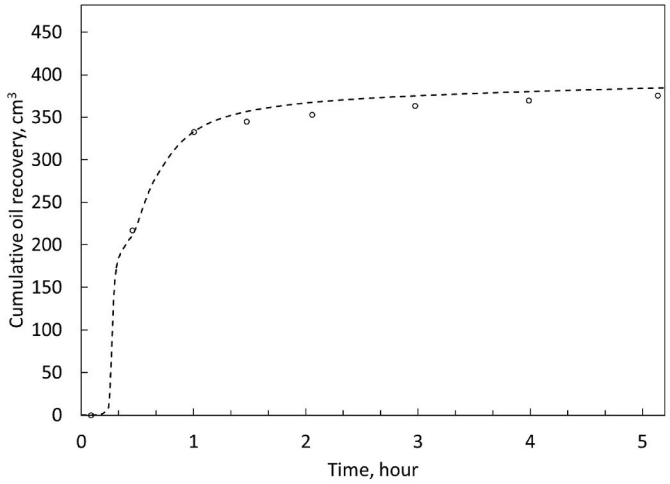


**Fig. 14.** Comparison of the SAGD oil production histories from the experiment and the simulation.

medium. The molecular diffusion is omitted in our case since molecular diffusion is negligible compared to dispersion as will be explained later. $D_{input}$ is equal to dispersivity, α, multiplied by interstitial velocity, $\frac{u}{\varphi}$.

In equation (2), $D_{num}$ is the numerical dispersion coefficient:

$$D_{num} = \left(\frac{u}{\varphi}\right)\frac{\Delta z}{2}[1 - N_{co}] \tag{4}$$

where u is Darcy velocity, Δz is the grid block size in the z-direction, and $N_{co}$ is the Courant number, which indicates the number of cells or fraction of a cell the solvent advances in one timestep.

$$N_{co} = \left(\frac{u}{\varphi}\right)\frac{\Delta t}{\Delta z} \tag{5}$$

If $\left(\frac{u\Delta t}{\varphi}\right) \ll \Delta z$, then $(1 - N_{co}) \approx 1$; $D_{num}$ becomes the following:

$$D_{num} = \left(\frac{u}{\varphi}\right)\frac{\Delta z}{2} \tag{6}$$

The numerical dispersion is calculated based on equation (6), and the maximum numerical dispersivity is 50% of the grid block size in the direction of the velocity for a one-dimensional system.

For our two-dimensional system, the numerical dispersion becomes the following (Russell and Wheeler, 1983):

$$D_{num} = \frac{|u_x|}{\varphi}\frac{\Delta x}{2} + \frac{|u_z|}{\varphi}\frac{\Delta z}{2} \tag{7}$$

where Δx and Δz are the gridblock sizes in the x and z directions, respectively, and $u_x$ and $u_z$ are Darcy velocities in the x and z directions, respectively. In these experiments, Δx and Δz are approximately equal. However, $u_z$ is about 15 times greater than $u_x$, and for simplicity, the numerical dispersion in the x-direction is neglected. Thus, equation (7) becomes

$$D_{num} = \frac{|u_z|}{\varphi}\frac{\Delta z}{2} \tag{8}$$

When equation (8) is used to solve the numerical dispersion in 2-D, it tends to underestimate the actual dispersion coefficient (Russell and Wheeler, 1983). However, the underestimation of numerical dispersion caused by using equation (8) is minuscule for our research cases mainly because $u_x$ was much smaller than $u_z$. Since our grid block size in the z-direction is 0.24 cm, the maximum numerical dispersivity would be 0.12 cm. By adding both numerical and input dispersion coefficients, the total dispersion coefficient was determined for each SA-SAGD case and shown in Table 10. The total dispersion coefficient was determined to be 0.093 $m^2$/day for $C_8$-SAGD and 0.012 $m^2$/day for $C_4$-SAGD. This is achieved by carefully fine-tuning input parameters in SA-SAGD simulations to history match the temperature distributions and oil production profiles shown in Section 3. Lastly, we can convert the total dispersion coefficients to dispersivities by dividing them by their interstitial velocities (Table 11). The estimated dispersivities have the same order of magnitude according to the scale of experiments. The difference likely reflects their different flow regimes. Analysis of simulation results implied that the $C_8$-SAGD experiment was affected by the thermal effect on the oil viscosity more than the $C_4$-SAGD experiment.

Hydrodynamic dispersion comprises molecular diffusion and mechanical dispersion (Lake, 1989; Pickens and Grisak, 1981). Molecular diffusion is the spreading of the solute particle caused by concentration gradients, while mechanical dispersion is mixing resulting from velocity variation along and across streamlines within the pore space.

If the flow velocity is small, there might be time for diffusion to act in the mass transfer process. On the other hand, if the velocity is large enough, there would be insufficient time for diffusions to equalize the concentration for a given pore space (Meng et al., 2018). According to Perkins and Johnston (1963) and Meng et al. (2018), one can calculate the pore-scale Péclet number as follows:

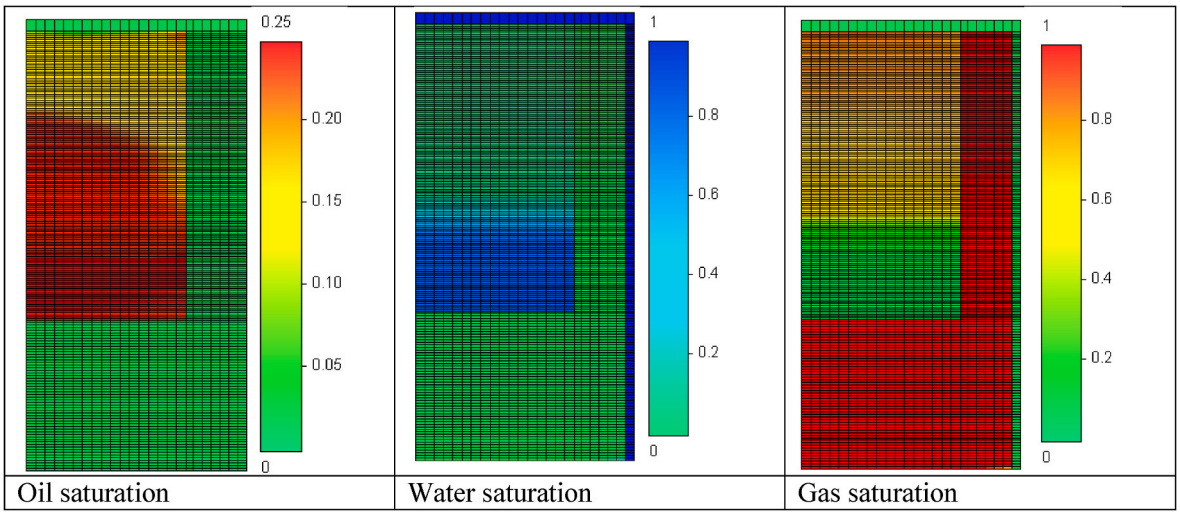


**Fig. 15.** SAGD saturation profiles at the end of the 5-h experiment.

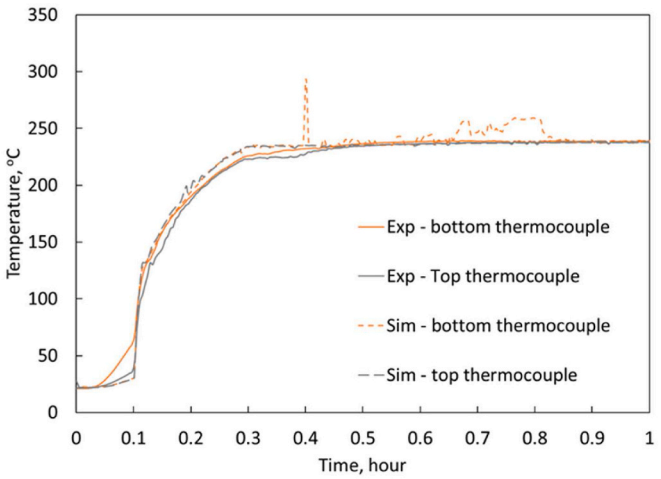


a) Temperature in the annular void space

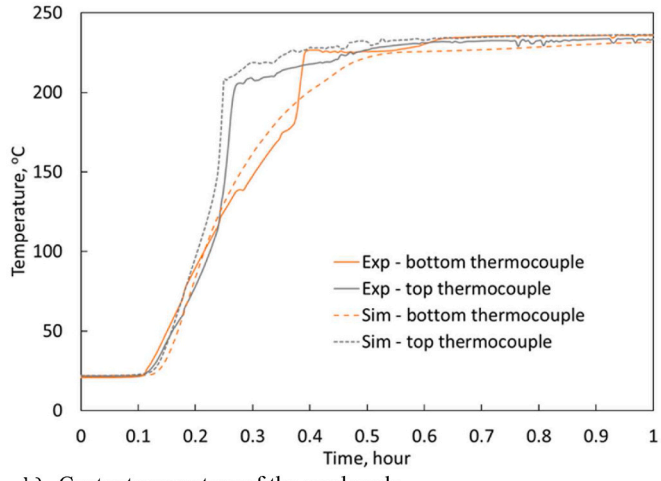


b) Center temperature of the sand pack

**Fig. 16.** Comparison of the $C_8$-SAGD temperature histories from the experiment and the simulation.

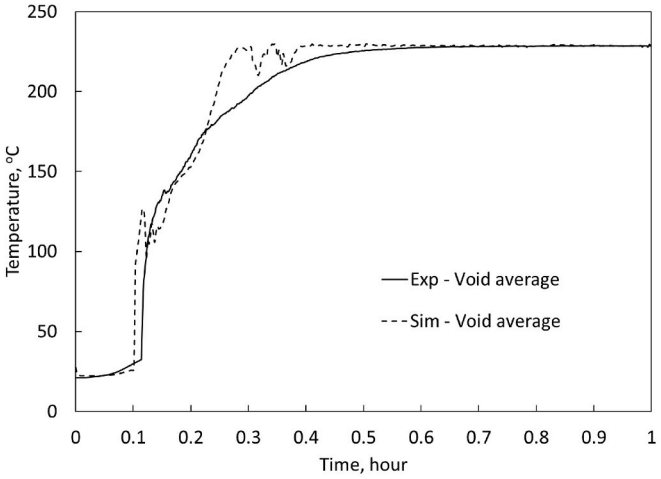


a) Temperature in the annular void space

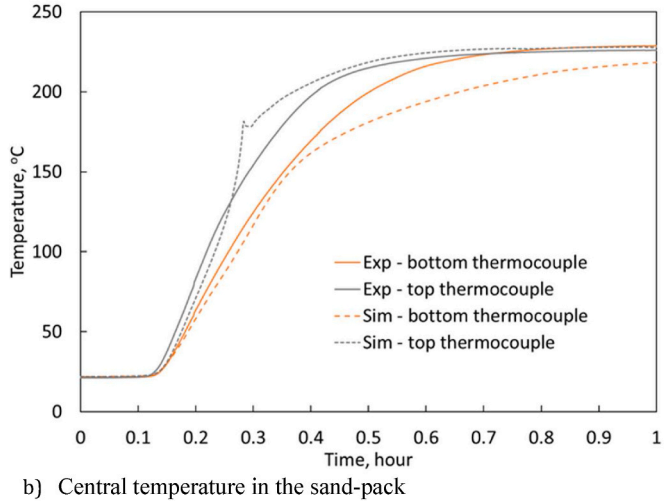


b) Central temperature in the sand-pack

**Fig. 17.** Comparison of the $C_4$-SAGD temperature histories from the experiment and the simulation.

$$N_p = \frac{v d_p}{D_o} \tag{9}$$

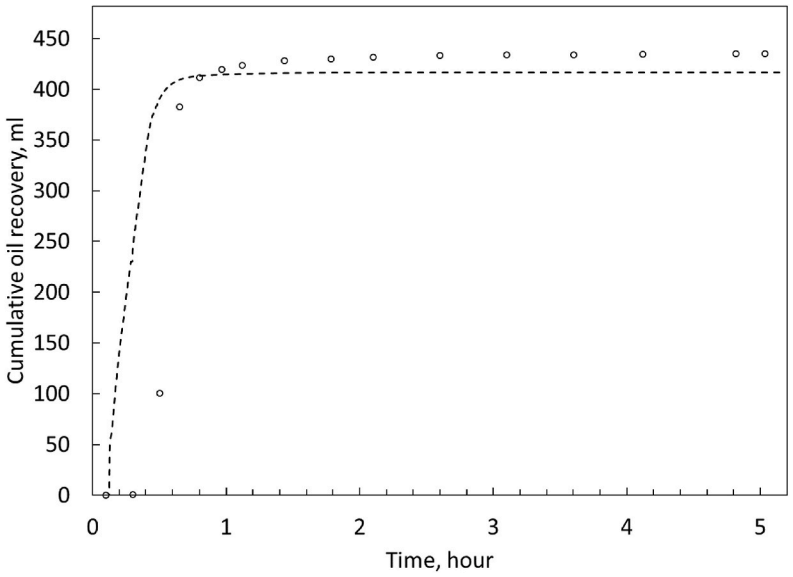


(a) Oil recovery. Experimetal data are shown as dots, and the simulated oil recovery is shown by the dashed line. As described in Section 2.6, the produced bitumen had not been fully recovered from the second and third drainage of the bottom producer. The history matching relied more on temperature data than these initial data points of oil recovery.

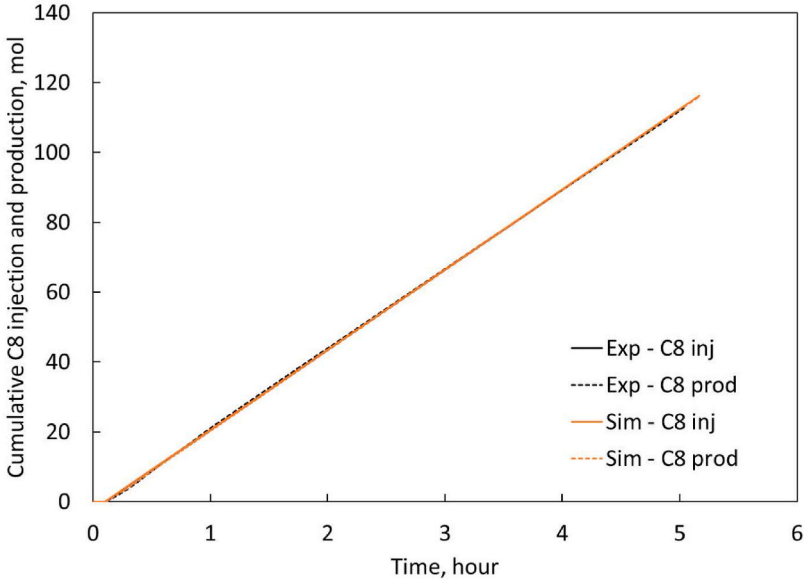


(b) $C_8$ injection and recovery. Experimental and simulation results are in good agreement.

**Fig. 18.** Comparison of the $C_8$-SAGD oil recovery and solvent injection/production histories from the experiment and the simulation.

where $\nu$ is interstitial velocity, $d_p$ is grain size, and $D_o$ is diffusion coefficient. If the Péclet number is much larger than $10^{-2}$ in the context of a solvent bitumen system (Russell and Wheeler, 1983), then dispersion will dominate, and diffusion can be neglected.

For the $C_4$-SAGD case, the Péclet number is calculated as follows:

$$N_p = \frac{vd_p}{D_o} = \frac{(8.87\ m/day)(5 \times 10^{-4}\ m)}{6.05 \times 10^{-5}\ m^2/day} = 73 > 10^{-2}$$

where the interstitial velocity was calculated to be 0.62 cm/min (8.87 m/day) when bitumen recovery was 150 ml, the grain size is 500 μm for $C_4$-SAGD, and molecular diffusion of $6.05 \times 10^{-5}$ $m^2$/day for $C_4$ from Zhao et al. (2018). The following Peclet number is calculated for $C_8$-SAGD:

$$N_p = \frac{vd_p}{D_o} = \frac{(17.32\ m/day)(5 \times 10^{-4}\ m)}{2.56 \times 10^{-5}\ m^2/day} = 338 > 10^{-2}$$

where the interstitial velocity was calculated to be 1.20 cm/min (17.32 m/day) when bitumen recovery was 150 ml, and the diffusion coefficient for $C_8$ in bitumen is $2.56 \times 10^{-5}$ $m^2$/day from Guerrero-Aconcha (Guerrero Aconcha and Kantzas, 2009). The calculated Péclet number ($N_p$) for $C_4$-SAGD and $C_8$-SAGD cases are 73 and 338, respectively. The calculated $N_p$ value is much larger than $10^{-2}$. That is, the mass transfer process in this experiment is dispersion dominant (i.e., not diffusion dominant).

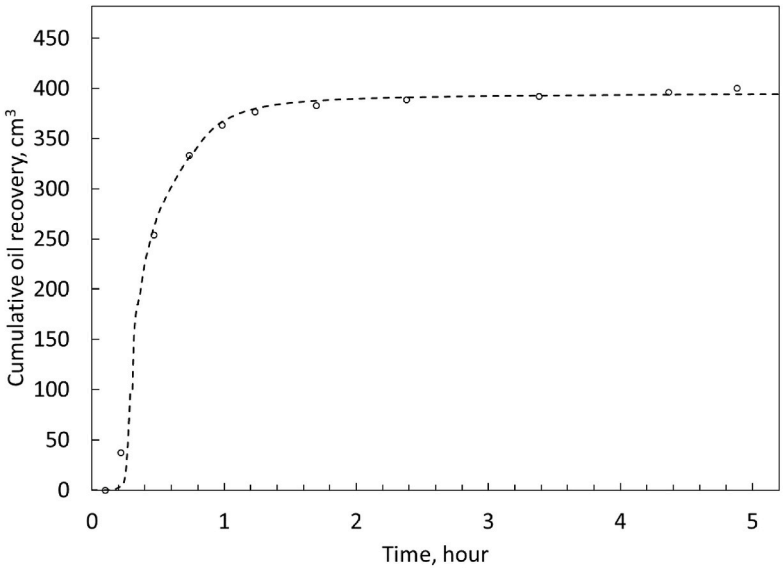


(a) Oil recovery. Dots and curve represent experimental data and simulation result, respectively.

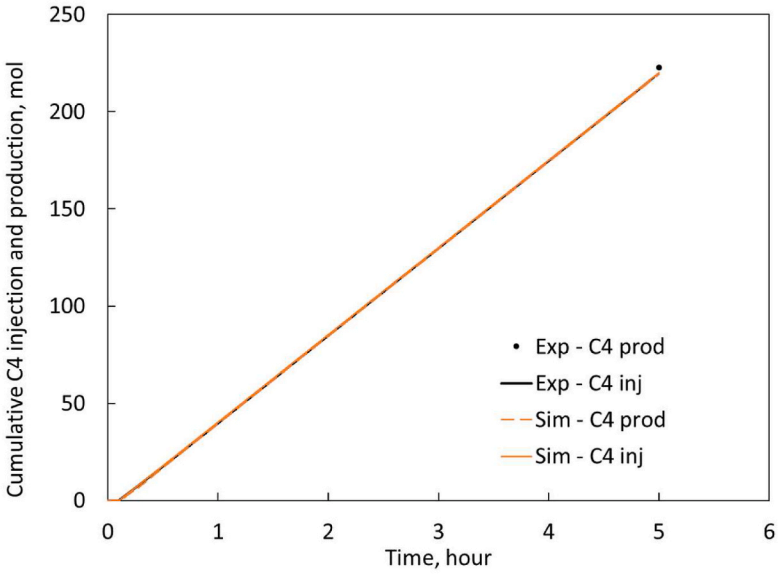


(b) $C_4$ injection and recovery. There was no continuous $C_4$ production history, and only a production value at the end of the experiment is shown as a black dot. The $C_4$ production was estimated using wet gas meter readings, and the estimation was 1.4% greater than the injected amount.

**Fig. 19.** Comparison of the $C_4$-SAGD oil recovery and solvent injection/production histories from the experiment and the simulation.

Much smaller velocities are used for similar lab-scale experiments conducted in the literature (Lim et al., 1996; Etminan et al., 2011). Etminan et al. (2011) reported a diffusion coefficient for a propane-bitumen system under the VAPEX process. Their calculated Péclet number was

$$N_p = \frac{vd_p}{D_o} = \frac{(3.541 \times 10^{-3}\ m/day)(2 \times 10^{-4} m)}{9 \times 10^{-5}\ m^2/day} = 7.87 \times 10^{-3} < 10^{-2}$$

where the average velocity was 0.014756 cm/h ($3.541 \times 10^{-3}$ m/day) and the grain size was 200 μm. The calculated Péclet number is still not large enough to neglect diffusion, and the mass transfer mechanism in the experiments is diffusion dominant. Therefore, the calculated coefficient is not well isolated as diffusion coefficient or dispersion coefficient.

In a realistic field-scale of SA-SAGD with a typical chamber edge velocity of 0.15 m/day (Venkatramani and Okuno, 2018b) and a typical grain size of 300 μm, the Péclet number will be

$$N_p = \frac{vd_p}{D_o} = \frac{(0.15\ m/day)(3 \times 10^{-4}\ m)}{6.05 \times 10^{-5}\ m^2/day} = 7.44 \times 10^{-1} > 10^{-2}$$

In field-scale, therefore, velocities are large enough to reach a dispersion dominant regime beyond diffusion dominant regime.

From this analysis, the interstitial velocity in lab experiments must be set in the range of 0.1 m/day or greater so that it can be away from the diffusion-dominant regime. From the calculated Péclet number, it is reasonable to assume that molecular diffusion was negligible in our SA-SAGD experiments.

Dispersivity and dispersion coefficient are both scale-dependent variables (Lake, 1989). Dispersivity on a field scale often reflects reservoir heterogeneity, such as the result of shale barriers. Meanwhile,

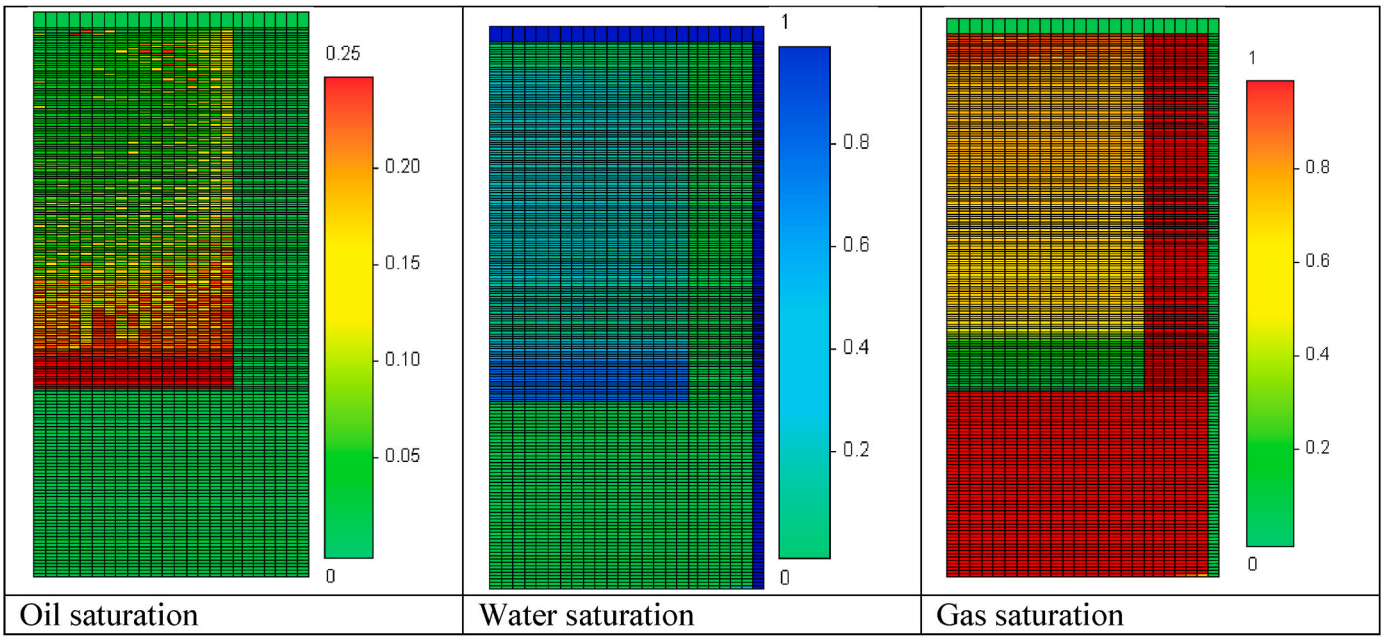


**Fig. 20.** $C_8$-SAGD saturation profiles at the end of the 5-h experiment.

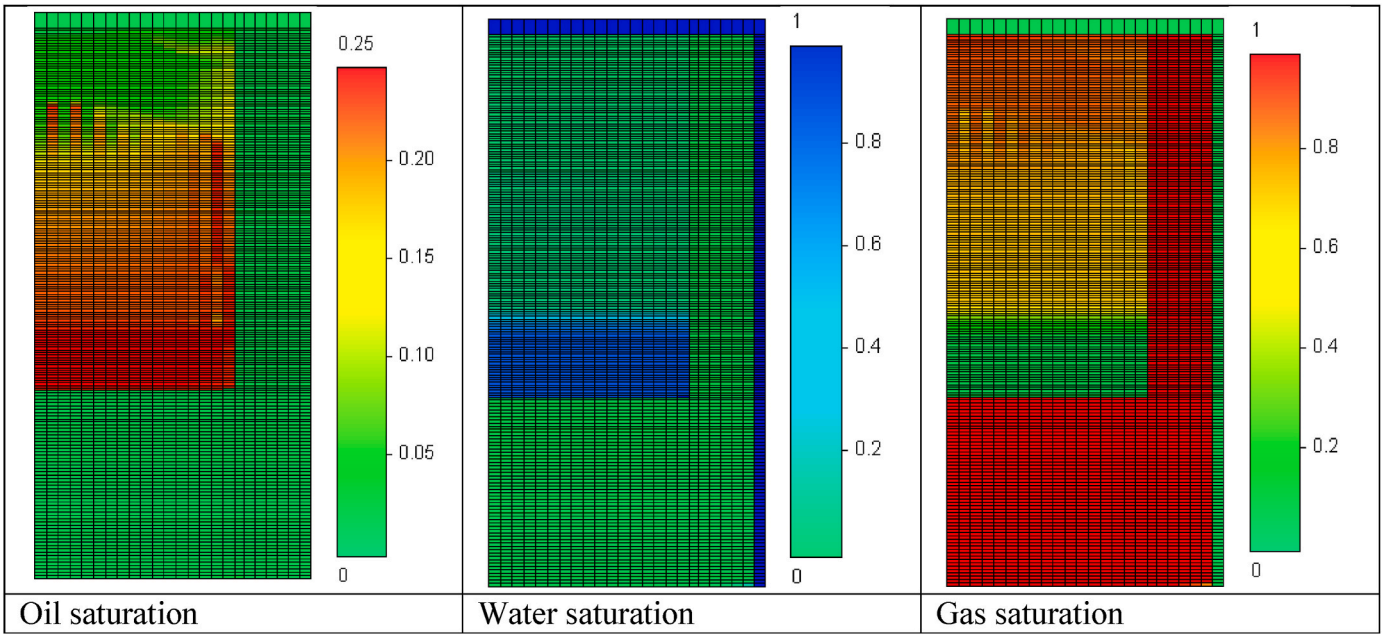


**Fig. 21.** $C_4$-SAGD saturation profiles at the end of the 5-h experiment.

lab-scale dispersivity mainly reflects the pore-scale tortuosity (Bear, 1972). The dispersion coefficients found in this experiment reflect the mixing characteristics of solvent at the pore scale. That is, upscaling of the dispersion coefficient is required for field-scale simulation of SA-SAGD. The dispersivities obtained for the $C_4$-SAGD and $C_8$-SAGD experiments based on the calibrated simulation models are consistent with the result of John et al. (John et al., 1134), who compiled data in the literature to show the growth of dispersivity with the distance traveled (Fig. 2 in their paper).

During our dispersion coefficient determination process, we considered the input dispersion and numerical dispersion to obtain a reliable physical dispersion coefficient. After upscaling (e.g., based on John et al. (John et al., 1134)), the total dispersion coefficient can be applied in field-scale simulation and can guide the user in determining the appropriate gridblock size for field-scale simulation. Details of how to set gridblock sizes for a desired level of mixing can be found in Garmeh and Johns (Garmeh, 2010) and Adepoju et al. (2013), for example.

## 5. Conclusions

This paper presented a set of experiments for investigating the effects of the chamber conditions (pressure, temperature, and solvent/steam composition) on bitumen gravity drainage in SA-SAGD. It consisted of one SAGD experiment as the base case and two sets of SA-SAGD with 20 mol% $C_4$ and 10 mol% $C_8$ at 3500 kPa. The experimental data were history matched by a numerical simulation model. The calibrated simulation model for SA-SAGD determined apparent dispersion coefficients for $C_4$ and $C_8$. The new experimental program presented can be

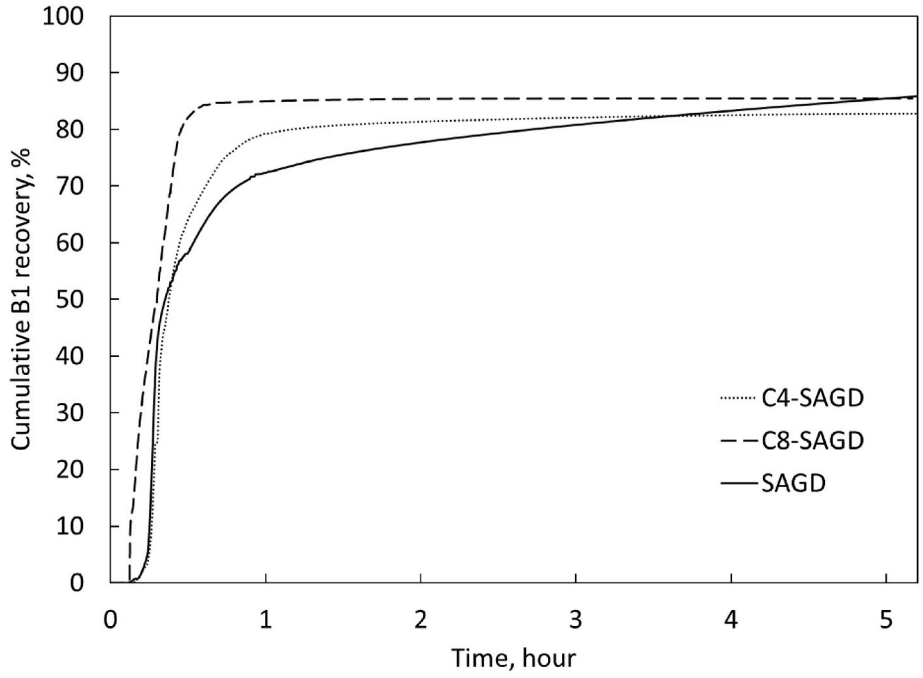


a) B1

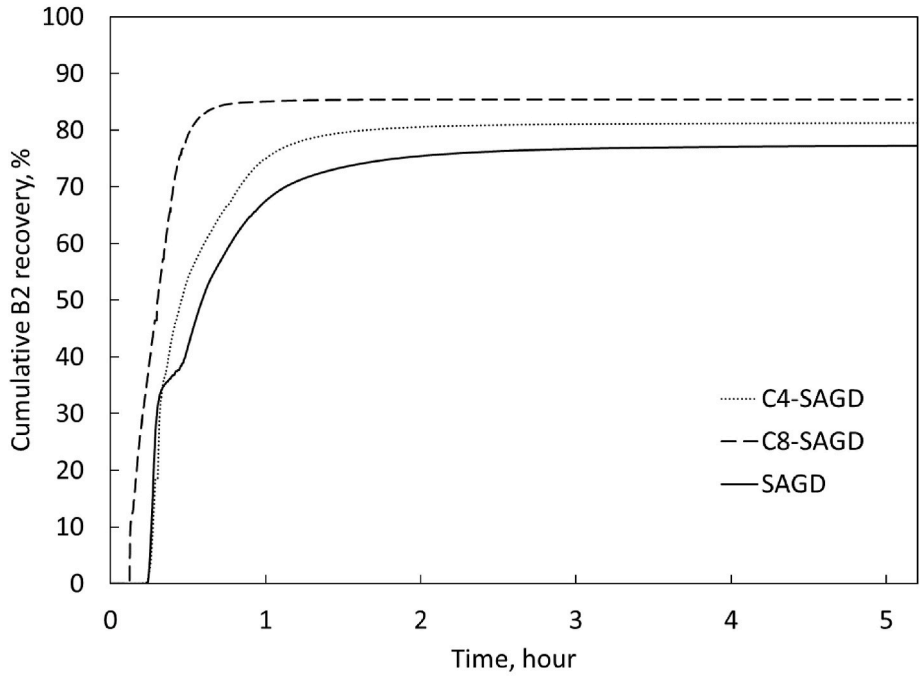


b) B2

**Fig. 22.** B1 and B2 oil component recovery factors for SAGD and SA-SAGD simulation cases.

used to quickly and systematically compare different solvent species for SA-SAGD in terms of condensation, bitumen dilution, and gravity drainage under given chamber conditions with a quantifiable level of dispersion. The main conclusions are as follows:

1. The experimental results showed the ultimate oil recovery was 78% with SAGD, 84% with $C_4$-SAGD, and 89% with $C_8$-SAGD. The peak rate was 9.8 $cm^3$/min with SAGD, 14.6 $cm^3$/min with $C_4$-SAGD, and 31.3 $cm^3$/min with $C_8$-SAGD. The $C_8$ solvent in $C_8$-SAGD was markedly more effective in enhancing the bitumen gravity drainage than $C_4$ in $C_4$-SAGD. The asphaltene content in the remaining oil was comparable between SAGD and $C_4$-SAGD, ranging from 22 to 26%. In $C_8$-SAGD, it ranged from 43 to 74% with a much smaller amount of remaining oil (Table 8).
2. Apparent dispersion coefficients were determined by history matching of SA-SAGD experimental data ($C_4$-SAGD and $C_8$-SAGD) using the numerical model calibrated with the SAGD experimental data. The dispersion coefficients of $C_4$ and $C_8$ for $C_4$-SAGD and $C_8$-

**Table 10**
Dispersion coefficients estimated for $C_8$-SAGD and $C_4$-SAGD.

| | Numerical dispersion, $cm^2$/min | Input dispersion, $cm^2$/min | Total dispersion, $cm^2$/min | Total dispersion, $m^2$/day |
|---|---|---|---|---|
| $C_8$-SAGD 10 mol % | 0.144 | 0.500 | 0.644 | 0.093 |
| $C_4$-SAGD 20 mol % | 0.074 | 0.010 | 0.084 | 0.012 |

**Table 11**
Dispersivities estimated for $C_8$-SAGD and $C_4$-SAGD.

| | Numerical dispersivity, cm | Input dispersivity, cm | Total dispersivity, cm |
|---|---|---|---|
| $C_8$-SAGD 10 mol% | 0.120 | 0.416 | 0.536 |
| $C_4$-SAGD 20 mol% | 0.120 | 0.024 | 0.144 |

SAGD were 0.012 $m^2$/day and 0.093 $m^2$/day, respectively, under the experimental conditions in this research. The difference between the dispersion coefficients comes from a large difference in interstitial velocity for the two cases. The estimated dispersivities for the two cases had the same order of magnitude according to the scale of experiments (0.536 cm for $C_8$-SAGD and 0.144 cm for $C_4$-SAGD). A potential reason for the difference between the estimated dispersivities is that the thermal effect on the oil viscosity affected the $C_8$-SAGD experiment more than the $C_4$-SAGD experiment.

3. It is important to ensure that the interstitial velocity of the small-scale experiment be sufficiently large so that the dispersion is dominant over the diffusion. For the small-scale SA-SAGD experiments in this research, the interstitial velocities had the order of 10 m/day. The solvent mass transfer in the porous medium was confirmed to be dispersion dominant.

## Credit author statement

Kai Sheng: Data curation; Formal analysis; Investigation; Methodology; Validation; Visualization; Writing – original draft. Hassan Amer: Data curation; Investigation; Visualization; Writing – original draft. Young Liu: Data curation; Visualization; Writing – original draft. Ryosuke Okuno: Conceptualization; Formal analysis; Funding acquisition; Investigation; Methodology; Project administration; Resources; Supervision; Validation; Writing – original draft. Abdullah Al-Gawfi: Data curation; Formal analysis; Investigation; Methodology; Validation; Writing – review & editing. Petro Nakutnyy: Data curation; Formal analysis; Investigation; Methodology; Validation; Writing – review & editing. Kazunori Nakagawa: Funding acquisition

## Declaration of competing interest

The authors declare that they have no known competing financial interests or personal relationships that could have appeared to influence the work reported in this paper.

## Acknowledgments

We gratefully acknowledge Japan Canada Oil Sands Ltd. and China National Offshore Oil Corporation International Ltd. for sponsoring this research. Ryosuke Okuno holds the Pioneer Corporation Faculty Fellowship in the Hildebrand Department of Petroleum and Geosystems Engineering at The University of Texas at Austin.

## Nomenclature

*Abbreviations*

| | |
|---|---|
| SAGD | Steam-Assisted Gravity Drainage |
| SA-SAGD | Solvent-Aided Steam-Assisted Gravity Drainage |
| SOR | Steam-to-Oil Ratio |
| CMG | Computer Modelling Group |
| VAPEX | Vapor Extraction |
| EOS | Equation of State |
| BIP | Binary Interaction Parameter |
| CME | Constant Mass Expansion |
| CDE | Convection-Dispersion Equation |

*Greek*

| | |
|---|---|
| $\mu$ | Viscosity, cp |
| $\rho$ | Density, $kg/m^3$ |
| $\omega$ | Acentric factor |
| $\alpha$ | Dispersivity, cm or m |
| $\varphi$ | Porosity |
| $\nu$ | Interstitial velocity, cm/min |
| $\tau$ | Tortuosity |
| $\sigma$ | Interfacial tension, dynes/cm |

*Latin*

| | |
|---|---|
| $D_o$ | Diffusion, $m^2$/day |
| D | Dispersion, $m^2$/day |
| $N_b$ | Bond number |
| $N_p$ | Péclet number |
| u | Darcy flow velocity, $cm^3$/min |
| $d_p$ | Diameter of pore size, μm |
| $D_{input}$ | Input dipersion, $m^2$/day |
| $D_{num}$ | Numerial dipersion, $m^2$/day |
| $\Delta t$ | Time step size, s |
| $\Delta z$ | Gridblock size, cm |

## References

Adepoju, O.O., Lake, L.W., Johns, R.T., 2013. Investigation of anisotropic mixing in miscible displacements. SPE Reservoir Eval. Eng. 16 (1), 85–96. https://doi.org/10.2118/166390-PA.

Al-Murayri, M.T., Maini, B.B., Harding, T.G., Javad, Oskouei, 2016. Cracked naphtha coinjection in steam-assisted gravity drainage. Energy Fuel. 30 (7), 5330–5340. https://doi.org/10.1021/acs.energyfuels.5b02773.

Ayodele, O.R., Nasr, T.N., Beaulieu, G., Heck, G., June 2008. Laboratory experimental testing and development of an efficient low-pressure ES-SAGD process. In: Paper PETSOC-2008-184 Presented at the Canadian International Petroleum Conference, Calgary, Alberta. https://doi.org/10.2118/2008-184.

Bear, J., 1972. Dynamics of Fluids in Porous Media. Elsevier, New York.

Butler, R.M., 1994. Steam-assisted gravity drainage: concept, development, performance and future. J. Can. Petrol. Technol. 32 (2), 44–50. https://doi.org/10.2118/94-02-05. PETSOC-94-02-05.

Butler, R.M., Mokrys, I.J., 1991. A new process (VAPEX) for recovering heavy oils using hot water and hydrocarbon vapor. J. Can. Petrol. Technol. 30 (1), 97–106. https://doi.org/10.2118/91-01-09. PETSOC-91-01-09.

Butler, R.M., McNab, G.S., Lo, H.Y., 1981. Theoretical studies on the gravity drainage of heavy oil during in-situ steam heating. In: Paper Presented at the 29th Canadian Chemical Engineering Conference in Sarnia, Ontario, on October 1, 1979. https://doi.org/10.1002/cjce.5450590407.

Computer Modelling Group (CMG). STARS Version 2018 User's Guide. Computer Modelling Group, Calgary, Alberta, Canada.

Das SK. Diffusion and Dispersion in the Simulation of VAPEX Process. Presented at SPE International Thermal Operations and Heavy Oil Symposium, 1–3 November 2005, Calgary, Canada, 1-6. SPE-97924-MS. https://doi.org/10.2118/97924-MS.

Das, S.K., Butler, R.M., 1996. Diffusion coefficients of propane and butane in peace river bitumen. Can. J. Chem. Eng. 74, 985–992. https://doi.org/10.1002/cjce.5450740623.

Deng, X., Huang, H., Zhao, L., Law, D.H.-S., Nasr, T.N., 2010. Simulating the ES-SAGD process with solvent mixture in athabasca reservoirs. J. Can. Petrol. Technol. 49 (1), 38–46. https://doi.org/10.2118/132488-PA.

Dunn, S.G., Nenniger, E.H., Rajan, V.S.V., 1989. A study of bitumen recovery by gravity drainage using low-temperature soluble gas injection. Can. J. Chem. Eng. 67, 978–991. https://doi.org/10.1002/cjce.5450670617.

Etminan, S.R., Parnian, H., Brij, M., Chen, Z.X., May 2011. Molecular diffusion and dispersion coefficient in a propane-bitumen system: case of vapour extraction (VAPEX) process. In: Paper SPE-143633-MS Presented at the SPE EUROPEC/EAGE

Annual Conference and Exhibition, Vienna, Austria. https://doi.org/10.2118/143633-MS.
Gao, J., Okuno, R., Li, H.A., 2017. An experimental study of multiphase behavior for n-butane/bitumen/water mixtures. SPE J. 22 (3), 783–798. https://doi.org/10.2118/180736-PA.
Garmeh, G., 2010. Investigation of Scale Dependent Dispersivity and its Impact on Upscaling Miscible Displacement. Ph.D. dissertation. The University of Texas at Austin, Austin, TX.
Guerrero Aconcha, U.E., Kantzas, A., May 2009. Diffusion of hydrocarbon gases in heavy oil and bitumen. In: Paper SPE-122783-MS presented at the Latin American and Caribbean Petroleum Engineering Conference, Cartagena de Indias, Colombia. https://doi.org/10.2118/122783-MS.
Haddadnia, A., Zirrahi, M., Hassanzadeh, H., Abedi, J., 2018. Dimethylether-a promising solvent for ES-SAGD. In: SPE Canada Heavy Oil Technical Conference.
John AK, Lake WL, Bryant S, Jennings J Investigation of Mixing in Field-Scale Miscible Displacements Using Particle-Tracking Simulations of Tracer Floods With Flow Reversal. SPE J. 15 (3): 598–609. SPE-113429-PA. https://doi.org/10.2118/113429-PA.
Keshavarz, M., Okuno, R., Babadagli, T., 2014. Efficient oil displacement near the chamber edge in ES-SAGD. J. Petrol. Sci. Eng. 118, 99–113. https://doi.org/10.1016/j.petrol.2014.04.007.
Keshavarz, M., Okuno, R., Babadagli, T., 2015. Optimal application conditions for steam/solvent coinjection. SPE Reservoir Eval. Eng. 18 (1), 20–38. https://doi.org/10.2118/165471-PA. SPE-165471-PA.
Khaledi, R.R., Beckman, M.S., Pustanyk, K., Mohan, A., Wattenbarger, C., Dickson, J., Boone, T., June 2012. Physical modeling of solvent-assisted SAGD. In: Paper SPE-150676-MS Presented in SPE Heavy Oil Conference Calgary, Alberta, Canada. https://doi.org/10.2118/150676-MS.
Khalifi, M., Zirrahi, M., Hassanzadeh, H., Abedi, J., 2020. Concentration-dependent molecular diffusion coefficient of dimethyl ether in bitumen. Fuel 274, 117809. https://doi.org/10.1016/j.fuel.2020.117809.
Kumar, A., Okuno, R., 2016. A new algorithm for multiphase-fluid characterization for solvent injection. SPE J. 21 (5), 1688–1704. https://doi.org/10.2118/175123-PA. SPE-175123-PA.
Lake, L.W., 1989. Enhanced Oil Recovery. Prentice Hall Inc, New Jersey.
Li, W., Mamora, D., Li, Y., 2011a. Light- and heavy-solvent impacts on solvent-aided-SAGD process: a low-pressure experimental study. J. Can. Petrol. Technol. 50 (4), 19–30. https://doi.org/10.2118/133277-PA.
Li, W., Mamora, D., Li, Y., 2011b. Solvent-type and ratio impacts on solvent-aided SAGD process. SPE Reservoir Eval. Eng. 14 (3), 320–331. https://doi.org/10.2118/130802-PA.
Lim, G.B., Kry, R.P., Harker, B.C., Jha, K.N.N., 1996. Three-dimensional scaled physical modelling of solvent vapor extraction of Cold Lake bitumen. J. Can. Petrol. Technol. 35 (4), 32–40. https://doi.org/10.2118/96-04-03. PETSOC-96-04-03.
Meng, L., Ji, D., Dong, M., 2018. Experimental and numerical study of the convective mass transfer of solvent in the expanding-solvent SAGD process. Fuel 215, 298–311. https://doi.org/10.1016/j.fuel.2017.11.028.
Moghadam, S., Nobakht, M., Gu, Y., 2009. Theoretical and physical modeling of a solvent vapor extraction (VAPEX) process for heavy oil recovery. J. Petrol. Sci. Eng. 65, 93–104. https://doi.org/10.1016/j.petrol.2008.12.029.
Nasr, T.N., Beaulieu, G., Golbeck, H., Heck, G., 2003. Novel expanding solvent-SAGD process "ES-SAGD". J. Can. Petrol. Technol. 42 (1), 13–16. https://doi.org/10.2118/03-01-TN.
Nghiem, L.X., Kohse, B.F., Sammon, P.H., 2001. Compositional simulation of the VAPEX process. J. Can. Petrol. Technol. 40, 54–61. https://doi.org/10.2118/01-08-05. PETSOC-01-08-05.
Perkins, T.K., Johnston, O.C., 1963. A review of diffusion and dispersion in porous media. SPE J. 3 (1), 70–84. https://doi.org/10.2118/480-PA. SPE-480-PA.
Pickens, J.F., Grisak, G.E., 1981. Modeling of scale-dependent dispersion in hydrogeologic systems. Water Resour. Res. 17 (6), 1701–1711. https://doi.org/10.1029/WR017i006p01701.
Russell TF, Wheeler MF. Finite Element and Finite Difference Methods for Continuous Flows in Porous Media. In The Mathematics of Reservoir Simulation 1983 CH2, 35–106. Society for Industrial and Applied Mathematics. https://doi.org/10.1137/1.9781611971071.
Sheng, K., 2016. Analysis of Phase Behavior for Steam-Solvent Coinjection for Bitumen Recovery. M.Sc. Thesis. University of Alberta.
Sheng, K., 2021. Interplay of Multicomponent Phase Behavior and Flow in Steam-Solvent Coinjection for Heavy-Oil and Bitumen Recovery. PhD Dissertation. University of Texas at Austin.
Sheng, K., Okuno, R., Al-Gawfi, A., Nakutnyy, P., Imran, M., Nakagawa, K., 2021a. An experimental study of steam-solvent coinjection for bitumen recovery using a large-scale physical model. SPE J. 1–18. https://doi.org/10.2118/205158-PA. SPE-205158-PA.
Sheng, K., Okuno, R., Imran, M., Yamada, T., 2021b. An experimental study of steam-assisted gravity drainage. SPE J. 26 (3), 1515–1534. https://doi.org/10.2118/200867-PA.
Shrivastava, V.K., 2003. Physical Dispersion in Compositional Reservoir Simulation. Ph. D. dissertation from the University of Calgary, Calgary, Alberta, Canada.
Venkatramani, A., 2014. Modeling of Water-Containing Reservoir Oil for Steam Injection Simulation. Master Thesis from the University of Alberta, Alberta, Canada.
Venkatramani, A., Okuno, R., 2018a. Mechanistic simulation study of expanding-solvent steam-assisted gravity drainage under reservoir heterogeneity. J. Petrol. Sci. Eng. 169, 146–156. https://doi.org/10.1016/j.petrol.2018.04.074.
Venkatramani, A., Okuno, R., 2018b. Steam-oil ratio in steam-solvent coinjection simulation for homogeneous and heterogeneous bitumen reservoirs. J. Energy Resour. Technol. 140 (11) https://doi.org/10.1115/1.4040529, 112903-112903-17.
Yang, C., Gu, Y., 2006. Diffusion coefficients and oil swelling factors of carbon dioxide, methane, ethane, propane, and their mixtures in heavy oil. Fluid Phase Equil. 243 (1), 64–73. https://doi.org/10.1016/J.FLUID.2006.02.020.
Yazdani, J., Maini, B., 2005. Effect of drainage height and grain size on production rates in the vapex process: experimental study. SPE Reservoir Eval. Eng. 8 (3), 205–213. https://doi.org/10.2118/89409-PA. SPE-89409-PA.
Zhao, H., Pierobon, S., Pettigrew, A., Doan-Prevost, J., Garnier, O.F., De Haas, T., November 2018. Measurement of propane and butane diffusion into heavy oil using microfluidics - is small better?. In: Paper SPE-193015-MS Presented at the Abu Dhabi International Petroleum Exhibition & Conference, Abu Dhabi, UAE https://doi.org/10.2118/193015-MS.
Zirahi, A., Yamchi, H.S., Haddadnia, A., Zirrahi, M., Hassanzadeh, H., Abedi, J., 2020a. 2-D physical model experimental study of ethyl acetate and steam Co-injection for in-situ bitumen recovery. Fuel 265, 116943. https://doi.org/10.1016/j.fuel.2019.116943.
Zirahi, A., Sadeghi Yamchi, H., Haddadnia, A., Zirrahi, M., Hassanzadeh, H., Abedi, J., 2020b. Ethyl acetate as a bio-based solvent to reduce energy intensity and CO2 emissions of in situ bitumen recovery. AIChE J. 66 (2), 16828. https://doi.org/10.1002/aic.16828.